AD-A046 050 COLORADO UNIV BOULDER DEPT OF ELECTRICAL ENGINEERING F/G 12/2
A SYNTHESIS THEORY FOR A CLASS OF MULTIPLE-LOOP SYSTEMS WITH PL--ETC(U)
1977 I HOROWITZ, T WANG AFOSR-76-2946

UNCLASSIFIED AFOSR-TR-77-1222 NL

1 OF 1
ADA
046050

END
DATE
FILMED
11-77
DDC

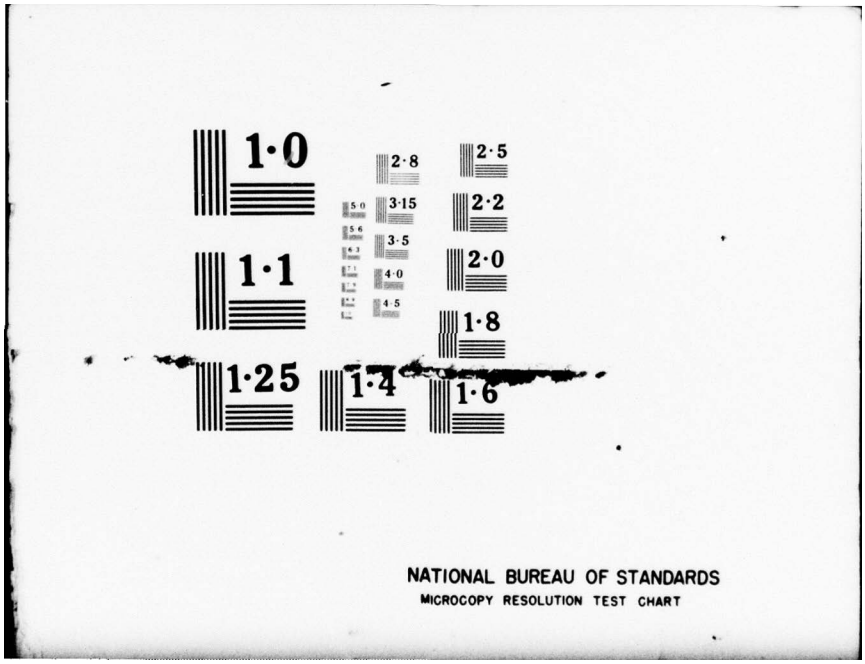
1·0
1·1
1·25
2·8
3·15
3·5
4·0
4·5
5·0
5·6
1·4
2·5
2·2
2·0
1·8
1·6
NATIONAL BUREAU OF STANDARDS
MICROCOPY RESOLUTION TEST CHART

AFOSR-TR- 77-1222

A SYNTHESIS THEORY FOR A CLASS OF MULTIPLE-LOOP SYSTEMS WITH PLANT UNCERTAINTY

Isaac Horowitz*† Te-Shing Wang*

ABSTRACT

There is given a single input-output linear, time-invariant plant with large parameter uncertainty consisting of two parallel branches, one of which has n internal sensing points. The objective is to satisfy specified frequency domain bounds on the system response to commands and disturbances over the parameter range, and to do so with sensibly minimum net effect at the plant input, of the n + 1 sensor noise sources. The basic problem is how to best divide the feedback burden among the n + 1 available feedback loops L_i. The procedure developed has high transparency,

---

* Department of Applied Mathematics, Weizmann Institute of Science, Rehovot, Israel.

† Department of Electrical Engineering, University of Colorado, Boulder, Colorado

This research was supported in part by the Air Force Office of Scientific Research under Grant No. AFOSR-76-2946 at the University of Colorado.

giving early perspective on the loop bandwidths, permitting approximate loop trade-offs without a detailed design. While the development is more difficult than in the single cascaded plant system, the procedure and final results are very similar: Each L_i has only one distinct frequency range say ω_i, in which there is trade-off between L_i and L_{i+1}, and $\omega_{i+1} > \omega_i$ with steadily increasing loop bandwidths going backwards from plant output to input. It is shown that for a class of problems the sensor noise effects can be tremendously reduced, when compared to an optimum single-loop design satisfying the same specifications.

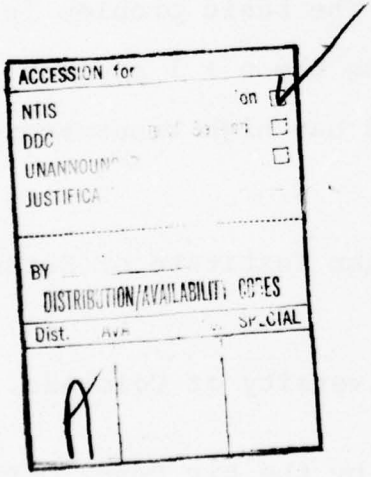

NOMENCLATURE

a_i	lower bound of k_i (following 4)
A_1, A_2	bounds on $\|T(j\omega)\|$ (1, Fig. 2)
b_i	upper bound of k_i (following 4).
$B_i(\omega)$	bounds on $L_{io}(j\omega)$ (Fig. 3, II Design example)
B_{iH}	hf boundary on L_{io} (6b, 7, Fig. 3)
$BW(L_i)$	bandwidth of L_{io} (IV)
C_i	output of P_i (Fig. 1)
C_D	system output due to D (Fig. 1)
D_i	disturbance input (Fig. 1)
$\mathcal{D}_i$	system function (3, 8)
e_i	excess of poles over zeros (before 4)
F	prefilter (Fig. 1)
g_i	system function (4)
G_i	compensation function (Fig. 1)
hf	high-frequency (range) (following 3)
I_{ij}	j = A,B,C,; i = 1,2..significant ω intervals of L_{io} (7, Fig. 4)
k_i	$i \neq e$, hf parameter (4)
k_e^j	effective hf parameter (4, 6)
L_i, L_i^o	loop transmission (3, 6, Fig. 4)
L_{io}	nominal value of L_i (II Design example, Fig. 4)
L_{io}^*	L_{io} for $\lambda_i > \lambda_{imax}$ (Fig. 3, IV)
LSVF	linear state variable feedback (I)
m_i	$= \|L_i\|$ (Fig. Alb)

M_i	$= \left\lvert \frac{L_i}{1 + L_i} \right\rvert$ (2, Fig. 3)
N_i	sensor noise input (Fig. 1)
o	as sub indicates nominal (Fig. 4)
P_i, P_{io}	ith plant section (Fig. 1)
P_e^j, P_e^{j*}	effective plant (3, 6, 12, Al, Fig. 1)
R	system command input (Fig. 1)
S	as sub indicates single loop (II, Fig. 4)
T	system transfer function (1)
$\mathcal{V}$	variation of a set (5, 9, 12)
X	plant input (Fig. 1)
α	trade-off parameter (Fig. 3, IV)
γ	bound on M (2, Fig. 3)
λ_i	$= P_i/P_{io}$ (9, 12)
ω	frequency radians per sec.
ω_{ij}	i = 1,2,... significant ω values of L_{io} (7, Figs 3, 4)
$\omega_{i\pi}$	ω at which Arg $L_{io} = -\pi$ (Fig. 7, Appendix 1)

A SYNTHESIS THEORY FOR A CLASS OF MULTIPLE-LOOP SYSTEMS WITH PLANT UNCERTAINTY

I. INTRODUCTION

There are two distinct approaches to the design of multiple-loop linear time-invariant systems. One of these LSVF (linear state-variable feedback), uses the optimal quadratic regulator solution and originally secured the desired system poles via a constant feedback gain matrix, driven by all the plant states [1, 2, 3 for bibliography.] Later refinements were observers for states which could not be sensed and of prefilters to obtain desired zeros [3, 4]. The problem of parameter uncertainty is being currently intensively researched using the concept of "robustness" [6-9]. LSVF is attractive because direct crank-turning gives a feedback design for a multiple-loop plant of any finite complexity, which has the desired poles at the nominal plant values and remains stable for sufficiently small parameter variations. A major shortcoming is that one cannot 'design to specifications' i.e., secure specified performance bounds over a given range of plant parameter values. Another is its complete neglect of the price paid for the benefits of feedback—the bandwidths of the loops. Thus, LSVF insists on a feedback structure even when there is exact knowledge of plant parameters and disturbances - a situation where feedback is not needed. In this sense LSVF is a continuation of classical network synthesis, using a different set of building blocks, because its primary purpose is pole-zero realization and only incidentally considers the uncertainty problem.

The second approach, denoted here as 'quantitative design' is characterized by (1) 'design to specifications' for significant plant uncertainty and disturbance attenuation. (2) emphasis on loop bandwidth minimization. So far, these have been secured only in terms of frequency response so it is often called the 'classical' approach, incorrectly because classical control theory almost completely overlooked both these problems. There is no crank-turning here, but purposeful design for sensitivity reduction. It has been developed only for the cascade plant structure [10], and to a certain extent for the multi-variable two matrix degree-of-freedom structure [11]. This need at present of separate development for different structures, compares unfavorably with LSVF generality. But in return there is highly economical design to specifications, and deep understanding of the feedback mechanism. Also, the concept of 'set equivalence' enables these techniques to be rigorously applied to large classes of linear and nonlinear uncertain time-varying systems with the same structures [12, 13]. This paper extends quantitative design to the cascade-parallel multiple-loop structure of Fig. 1.

Problem Statement

In Fig. 1 the P_i are transfer functions of sections of the uncertain plant and N_i are the sensor noise sources - drawn heavy to emphasize they are constrained and unalterable. There is independent uncertainty of the parameters of each P_i. Despite this uncertainty, the system frequency response to commands $T(j\omega) = C(j\omega)/R(j\omega)$ is to satisfy specified bounds

$$0 < A_1(\omega) \leq |T(j\omega)| \leq A_2(\omega) \qquad (1)$$

It has been shown that time-domain bounds on the output and its derivatives of any order [13] can be achieved by satisfying such ω-domain bounds. The problem is to find a sensibly optimum systematic means of dividing the 'feedback burden' among the $n + 1$ available loops. All the feedback signals go to the plant input X, because 'plant modification' [11] is assumed not allowed. Thus, in Fig. 1a, $X = C/P$ and each C_i is determined by X and the P_j, so the C_i needed to obtain a desired output C are independent of the G_i. This is not the case if feedback to internal plant variables is allowed.

Disturbance attenuation is another major reason for using feedback. To simplify the presentation, for the present the only requirement in Fig. 1 a, (with L defined by (3) later), is that $|C/D| = |(1+L)^{-1}| \leq$ some constant. It is more convenient [15] to use

$$M \triangleq \left|\frac{L}{1+L}\right| \leq \gamma \text{ a constant}, \quad \forall \ \omega. \tag{2}$$

Nonminimum-phase plants, unstable plants and the generality of the structure in Fig 1a, are postponed for later discussion, except to note that any $n + 2$ degree of freedom system structure [11] may be used e.g., Fig. 1b for the case $n = 2$.

The above is a very difficult problem, with very little treatment in general and none at all for Fig. 1. It obviously does not lend itself to a rigorous mathematical theorem-proving treatment. The approach taken is to find the principal design factors and trade-offs, based on the following design philosophy: The outer loop L from C may be designed to cope only with the uncertainty in P_b, P_c, which can give an L much more economical than in a single-loop design in which L must cope with all P. The first inner loop L_1 from C_1 may be designed to cope only with P_1, with possible great saving compared to an L_1 which

copes with $P_1P_2\cdots P_n$. Similarly the second inner loop need cope only with P_2, etc. The result is considerable transparency and insight, enabling the designer to decide how to divide the feedback burden among the loops.

Simplifications initially made in order to concentrate on the essentials, are covered in Sec. V.

II DESIGN OF OUTER LOOP

If the plant is minimum-phase and open-loop stable (1,2) are achieveable [15] with a single loop $G_i = 0$, $i = 1,..,n$, $G = G_S \neq 0$ in Fig. 1a. But the resulting $L_S = G_S P$ may then require very large bandwidth, causing great amplification of the sensor noise N, as in a later example - Fig. 5. The simplistic approach, later justified, is to therefore use the inner loops to ease, as much as possible, the outer loop burden. In Fig. 1a, let

$$P_a \triangleq P_n P_{n-1}\cdots P_2 P_1, \quad P \triangleq P_a P_b + P_c ,$$

$$\mathcal{D} \triangleq (1 + P_n G_n + P_n P_{n-1} G_{n-1} + \cdots\cdots P_n\cdots P_1 G_1) + PG$$

$$\triangleq \mathcal{D}_1 + P_G \triangleq \mathcal{D}_1(1+L), \quad L = \frac{PG}{\mathcal{D}_1} \triangleq P_e G. \qquad (3a\text{-}f)$$

$$T(s) = \frac{C(s)}{R(s)} = \frac{FGP}{\mathcal{D}} = \frac{FGP/\mathcal{D}_1}{1+(GP/\mathcal{D}_1)} = F\,\frac{L}{1+L} \quad .$$

$$-\frac{X}{N} = \frac{G}{\mathcal{D}} = \frac{G}{\mathcal{D}_1(1+L)} = \frac{L/P}{1+L}$$

In (3f) the sensor noise effect is examined at the plant input X where it tends to be large [16, and Fig 5 here], causing plant saturation. In the high-frequency range (denoted as hf), (3f) $\rightarrow L/P$ where $|L(j\omega)| << |$ but $|L/P|$ can be very large (Fig. 4), - the hf range is the major trouble source. Thus, in Fig. 5b the lowest ω range with large and

sharp peaking of $|X/N|$ is ~ 300 rps at which, from Fig. 4, the nominal $|L| \sim -46$db. Hence, the major effort in sensor noise effect minimization will be made in hf. Since P is constrained in (4), such minimization requires $|L|$ minimization. But from (3) L must cope with $P_e = P/\mathcal{D}_1$ uncertainty. Therefore, for maximum economy of L, choose the G_i, $i = 1,\ldots, n$ in $\mathcal{D}_1$ of (3c) to minimize the uncertainty in $P_e = P/\mathcal{D}_1$.

Consider accordingly the uncertainty in $P_e = \dfrac{P_1P_2\ldots P_nP_b+P_c}{1+P_nG_n+\ldots+P_n\ldots P_2P_1G_1}$ in hf where each $P_i \to k_i/s^{e_i}$, e_i the excess of poles over zeros of P_i. Since $P_1P_2..P_nP_b$ parallels P_c in Fig. 1, it is assumed that $(e_1+e_2+\ldots e_n) + e_b \triangleq e_a+e_b = e_c$. Hence, at hf

$$P_e = \frac{P}{\mathcal{D}_1} \to \frac{k_ak_b+k_c}{s^{e_c}[1+k_ng_n+..+k_ag_1]} \triangleq \frac{k_e}{s^{e_c}} \quad , \text{ where}$$

$$G_n \triangleq g_ns^{e_n},\ G_{n-1} \triangleq g_{n-1}s^{e_n+e_{n-1}},\ \ldots\ ,\ G_1 \triangleq g_1s^{e_a} \qquad (4a,b)$$

The range of k_i is taken as $[a_i,b_i]$, $b_i>a_i>0$. In the logarithmic complex plane (Nichols chart), P_e is not a point but a set $\{P_e\}$ because of the uncertainty. For any fixed $k_1,\ldots,k_n$ values the set $\{P_e\}$, due to $\{k_b\}$, $\{k_c\}$ in (4a), is a vertical line whose length, Lgth $\{P_e\} = \left[\dfrac{k_ab_b+b_c}{k_aa_b+a_c}\right]_{db}$ is a function of k_a, and is maximum at $k_a = a_a$ if $b_c/a_c \geq b_b/a_b$ (at b_a if $b_c/a_c \leq b_b/a_b$). The former is assumed because P_c is in parallel with P_aP_b - see Sec V.

Hence, due to <u>all</u> the k_i uncertainty sets $\text{Lgth}\{P_e\} \geq (a_a b_b + b_c)/(a_a a_b + a_c)$, with equality iff $\exists$ g_i such that the sets $\{k_e(k_a, k_b, k_c)\}$ of (4a) $\subseteq$ $\{k_e(a_a, k_b, k_c)\}$ as the k_i independently range over $[a_i, b_i]$. It is readily seen that such g_i exist e.g. $g_2 = \ldots = g_n = 0$, $b_b/b_c \leq g_1 \leq a_b/a_c$, compatible with the previous $b_c/a_c \geq b_b/a_b$. (In the case $b_c/a_c \leq b_b/a_b$ the analagous, compatible condition is $b_b/b_c \geq g_1 \geq a_b/a_c$). Thus, at hf the best the inner loops can do for the outer loop L, leads to it coping with a gain uncertainty set

$$\{a_a k_b + k_c\} \triangleq \mathcal{V} \circ \{P_e\} \quad , \quad \text{of}$$

$$\text{Lgth}\, \mathcal{V} \circ = \frac{a_a b_b + b_c}{a_a a_b + a_c} \tag{5a,b}$$

For example if $n = 2$, all $a_i = 1$, $b_i = 40, 10, 60, 200$ for $i = 1,2,b,c$ then in a single-loop design L_S must handle at hf $\{P\}$ of length $[(b_a b_b + b_c)/(a_a a_b + a_c)]_{db} = 81.7$ db whereas (5b) given 42.3db, a saving of 39.4db.

The hf region is most important for sensor noise, and the hf form of P_i in (4) greatly simplifies the problem there. But design of the outer loop requires the uncertainty set for the entire spectrum. The complexity of the calculations for general P_i with uncertain poles and zeros would obscure the important features, for the sake (Sec. V) of a minor point. Therefore, in the meantime let $P_j = k_j/s^j$ $j = a,b,c$ so (4,5) apply for all ω. Outer-loop design is now a single-loop problem with the equivalent plant P_e of (4a) denoted by

$$P_e^0 \triangleq \frac{P_{a0}P_b+P_c}{1+P_{no}G_n+\ldots+P_{no}\ldots P_{20}P_{10}G_1}$$

$$= \frac{a_a k_b+k_c}{(1+a_n g_n+\ldots+a_a g_1)s^{e_c}} \triangleq \frac{k_e^o}{s^{e_c}} \qquad (6a,b)$$

and $L^0 = P_e^0 G$

The super-oh on P_e, k_e, L indicates P, k_e, L with $P_1, P_2, \ldots P_n$ at their nominal values. The problem is to find G or equivalently a nominal $L_0^0 = P_{eo}^0 G$ so that (2) and $\Delta \ell n|T(j\omega)| \leq \ell n \frac{A_2(\omega)}{A_1(\omega)}$ of (1), are satisfied. The optimum design for this single-loop problem [16] is briefly reviewed here, with an example which is very helpful in explaining the multiple-loop design theory.

Design Example

In Fig. 1a let $n = 2$, $P_j = k_j/s$, $j = 1,2,b$; $P_c = k_c/s^3$; $a_1 = 20$, $a_2 = 50$, $a_b = 1$, $a_c = 1000$, $b_1 = 800$, $b_2 = 500$, $b_b = 60$, $b_c = 200{,}000$. The bounds $A_1(\omega)$, $A_2(\omega)$ of (1) are in Fig. 2, and $\gamma = 2.3$db in (2). The nominal plant values are taken as a_i (with no loss in generality) Note 1: The specifications must be consistent with physical reality i.e., it is crucial [16] that $\exists\, \omega_0$, such that for $\omega > \omega_0$, the largest variation of $P_e < \ell n \frac{A_2(\omega)}{A_1(\omega)}$, in order that no sensitivity reduction be needed at large enough ω, permitting $L(j\omega) \to 0$ as $\omega \to \infty$. From Fig. 2, $\omega_0 \approx 55$ for a multiple loop design, 280 for a single-loop design.

Design of Outer Loop

The procedure in [15] is followed. From (3a), $\Delta \ell n|T| = \ell n\left|\frac{L^0}{1+L^0}\right|$ $L^0 = P_e^0 G = k_e^0/s^{e_c}$ of (6) with k_e^0 uncertainty (5), equal to 42.3db. Hence in the Nichols chart, $\ell n\, L^0 = \ell n\, P_e^0 + \ell n\, G$ is any point on line AB in Fig. 3, of length 42.3db. By means of $G(j\omega)$ this vertical line which is the variation set $\mathcal{V}^0 = \mathcal{V}\{P_e^0\}$ can be translated, but not rotated to any region in the Nichols chart, giving the variation set of L^0, $\mathcal{V}\{L^0\}$, with the nominal $L_0^0 = GP_{e0}^0$ at A. Note that the nominal L of (3d), denoted by $L_0 \equiv L_0^0$ and the nominal P_{eo} of (3d) $\equiv P_{e0}^0$, justifying $G = L_0/P_{e0} = L_0^0/P_{e0}^0$.

For any ω say ω_1, one finds the boundary $B(\omega_1)$ of the set $L_0(j\omega_1)$ which satisfy (2) and $\ell n|T| \le \ell n \frac{A_2(\omega)}{A_1(\omega)}$. For example, in Fig. 3 at $\omega = 20$, X_1 is satisfactory for $L_0(j20)$ because the range of $M^0 \triangleq \left|\frac{L^0}{1+L^0}\right|$ is from A ($M^0 = -23.9$ db) to B ($M^0 = -.4$ db) giving the allowed 23.5 db for $\frac{A_2(20)}{A_1(20)}$. Similarly, at X_2 the variation is from -22.7 to .8 db. Any larger $|L_0|$ at the same Arg L_0 is satisfactory, but not smaller $|L_0|$. $B(20)$ is thus found. Due to (1) and Note 1 of Design Example, as $\omega \to \infty$ $B(\omega)$ would $\to$ a vertical line at -180° extending from -42.3 db to 0 db. But (2) gives the boundary B_H of Fig. 3 obtained by projecting the locus of $\left|\frac{L_0}{1+L_0}\right| = \gamma = 2.3$ db downward by 42.3 db. At small ω, e.g., $\omega = .5$, (1) dominates - see Fig. 3. At larger ω e.g., $\omega = 2$, 10, part of $B(\omega)$ is due to (1) and part is due to (2). There always exists ω_H such that for $\omega > \omega_H$, $B(\omega) = B_H$[15,16]. Here $\omega_H \sim 70$ rps. The generality of P at hf (4a) and of B_H lead to a general shape for $L_0(j\omega)$ (Fig. 3,4) in large hf uncertainty problems, as follows.

$L_0(j\omega)$ must satisfy $B(\omega)$ but (3f) at hf suggests $|L_0(j\omega)|$ be decreased as rapidly as possible vs ω. As $s \to \infty$, $L_0(s) \to k_L/s^{e_L}$. A reasonable definition of optimum L_0 is one satisfying the $B(\omega)$ with a minimum k_L for a fixed e_L. Such an optimum exists, is unique, lies on $B(\omega)$ at each ω and can be approximated as closely as desired by a rational function [16]. There is trade-off between complexity of the rational $L_0(s)$ and k_{Lmin}, so a practical sensibly optimum $L_0(j\omega)$ is as shown in Figs. 3,4. The shape and length of B_H are important. $L_{0,opt.}$ tries to decrease $|L_0|$ rapidly vs ω, but in Fig. 3 B_H constrains min [Arg $L_0(j\omega)$] $\geq -130°$, with corresponding minimum average $d|L_0(j\omega)|/d\omega = -\frac{-130}{180}(40) \approx -29$db/decade [11]. Thus, $|L_0(j\omega)|$ must decrease rather slowly up to ω_x in Figs. 3,4 after which the permitted decrease of Arg $L_0(j\omega)$, at bottom of B_H, permits $|L_0(j\omega)|$ to decrease very rapidly.

This paper is devoted to problems where $\exists$ an $[\omega_d, \omega_z]$ interval in which the sensibly optimum $L_0(j\omega)$ has the shape shown in Fig. 3. Plants with uncertain highly underdampled pole-zero pairs (e.g. bending modes) could be included, if these occur at $\omega < \omega_d$ and/or $\omega > \omega_z$. However, the multiple-loop problem is complex enough without bending modes, so this class is omitted here.

It is seen from Figs. 3,4 that the hf uncertainty i.e. of k_e in (6), is the factor which can give large cost of feedback. This is because the length of B_H is that of $\{k_e\}$. On B_H, $|L_0|$ must decrease slowly vs ω while $|P_0|$ may decrease faster and at hf from (3f), $|X/N| \doteq |L_o/P_o|$ may then be $>> 1$ even though $|L_0| << 1$ (Figs. 4,5). Hence, it is desirable to minimize Lgth (B_H) = Lgth $\{k_e\}$. Use of an inner loop permits a maximum reduction of 39.4 db here. The saving in bandwidth is $\sim 40/29$ decades (L_{SO} ve L_0 in Fig. 4). The

reduction in sensor noise effect at X is enormous (Fig 5b), because the rms noise value is obtained by integrating arithmetic values on a airthmetic ω scale.

For later use, the following ω intervals in Fig. 3,4 are emphasized:

$$I_A \triangleq [0,\omega_x) \approx [0,90), \quad I_B \triangleq [\omega_x,\omega_z) \approx [90, 330)$$

$$I_C \triangleq [\omega_z, \infty) \approx [330, \infty). \tag{7}$$

The design of the first inner loop L_1 is decisively influenced by these intervals of the outer loop L_0.

III DESIGN OF INNER LOOPS

First Inner Loop L_1

In II the inner loops were apparently sacrificed, in order to obtain the most economical outer loop and thereby minimize the effect of sensor noise N at X. $G_2 = \ldots = G_n = 0$, $G_1 = s^{e_a} b_b/b_c$ were found satisfactory for this purpose. The obvious criticism is that this G_1, besides being impractical, would tremendously amplify hf N_1 noise effect at X (Fig. 1) and likely more than cancel the benefit gained for L. The answer is that while these G_i are satisfactory, there are other much smaller acceptable values. This is due to the mechanics of sensitivity reduction such that $L_0(j\omega_1)$ optimally designed to handle an uncertainty set $V(\omega_1)$ can in practice handle a set $V_y(\omega_1)$ much larger than $V(\omega_1)$ (e.g. Fig 8 of [10]). So, the next step is to find the bounds $B_1(\omega)$ on the first inner nominal loop $L_{10}(j\omega)$ such that the economical L_0 of II is satisfactory. The bounds on L_{10} are, in fact, very modest.

For this purpose (3c,f) are entended as follows. Let

$$\mathcal{D} = \mathcal{D}_1(1+L) = [(1+P_nG_n+\ldots+P_n\ldots P_2G_2) + P_aG_1](1+L) \triangleq (\mathcal{D}_2 + P_aG_1)(1+L)$$

$$\triangleq \mathcal{D}_2(1+L)(1+L), \qquad L_1 = \frac{P_aG_1}{\mathcal{D}_2}$$

$$-\frac{X}{N} = \frac{G_1}{\mathcal{D}} = \frac{G_1}{\mathcal{D}_2(1+L_1)(1+L)} = \frac{L_1/P_a}{(1+L_1)(1+L)} \qquad (8a\text{-}c)$$

$\doteq L_1/P_a$ in the crucial hf. Hence to minimize $|X/N_1|$ at fixed L, minimize $|L_1|$. But L_1 must cope with the uncertainty in $P_1, P_2, \ldots P_n$ ignored by L^0. However, if G_2 can cope with $P_2,\ldots,P_n$ then L_1 need only cope with P_1. L_1 is designed accordingly and denoted by L_1^0 to indicate its neglect of $P_2,\ldots,P_n$ uncertainty. So now, P_e^0 of (7a) is replaced by

$$P_e^1 \triangleq \frac{P_1P_{20}\ldots P_{no}P_b+P_c}{1+P_{no}G_n+\ldots+P_{no}\ldots P_{20}P_1G_1} = \frac{\lambda_1P_{ao}P_bP_c}{\mathcal{D}_{20}(1+\lambda_1L_{10})},$$

$$\lambda_1 \triangleq \frac{P_1}{P_{10}} \qquad (9a\text{-}c)$$

with $$\mathcal{V}^1 = \mathcal{V}\{P_e^1\} = \left\{\frac{\lambda_1a_ak_b + k_c}{1+\lambda_1L_{10}}\right\}$$

instead of $\mathcal{V}^0 = \{a_ak_b+k_c\}$ of (5a). In (9) L_{10} is the nominal $L_{10}^0 \equiv L_{10}$ (cf $L_0^0 \equiv L_0$) and $\mathcal{D}_{20} = \mathcal{D}_2$ at nominal P_{io}, for $i = 1,\ldots, n$.

L_0 was designed to handle P_e^0 with its $\mathcal{V}^0$, but now it must handle P_e^1 with its $\mathcal{V}^1 \supset \mathcal{V}^0$. What are the bounds $B_1(\omega)$ on $L_{10}(j\omega)$ so that the original L_0 remains satisfactory? This equestion may be answered by simple trying L_{10} values and checking if (1,2) are satisfied. It is found that the $B_1(\omega)$ are decisively influenced by the intervals I_A, I_B, I_C of L_0 in (7). The results are stated here and their explanation in Appendix 1.

Nature of $B_1(\omega)$ bounds on L_{10}

(1) For $\omega \in I_A = [0,90)$, $B_1(\omega)$ are upper bounds, i.e., $|L_{10}(j\omega)|$ must be < some value which is a function of $\text{Arg}L_{10}(j\omega)$ - Fig. 6a.

(2) For $\omega \in I_B = [90,330)$, $B_1(\omega)$ are lower ones precluding $L_{10} \equiv 0$ (Fig. 6b).

(3) For $\omega \in I_C = [330,\infty)$, $B_1(\omega)$ in Fig. 6b are closed curves in the Nichols Chart which tend to a vertical line B_{1H} of length $\left(\frac{b_1}{a_k}\right)_{db}$ at $\text{Arg}L_{10} = -\pi$.

Just as in the design of L_0, so the optimum L_{10} would lie on $B_1(\omega)$ at all ω but is in practice approximated by a rational function - Figs. 4,6. One may define intervals of L_{10} similar to I_A, I_B, I_C of L_0, i.e., in Figs. 4,6: $I_{1A} = [0,\omega_{1x}^-)$, $I_{1B} = [\omega_{1x}^-, \omega_{1x}^+)$, $I_{1C} = [\omega_{1x}^+,\infty)$. Here $I_{1B} \doteq 0$ because B_{1H} has zero width. In practice, one would likely (in addition to (2)), assign bounds in Fig. 1, on

$$\frac{C_i}{D_i} = \frac{1}{(1+L)(1+L_1)\ldots(1+L_i)} \tag{10}$$

leading to finite-width B_{iH} and larger I_{iB}. Such finite B_{iH} are easily added in Figs. 6,7, but are omitted here for simplicity.

Second Inner Loop L_2

The above discussion is repeated for L_2, but now P_2 uncertainty is included with (8) extended to

$$\mathcal{D} = \mathcal{D}_2(1+L_1)(1+L) = [(1+P_nG_n+\ldots+P_n\ldots P_3G_3) + P_n\ldots P_2G_2](1+L_1)(1+L)$$

$$\triangleq (\mathcal{L}_3 + P_n\ldots P_2G_2)(1+L_1)(1+L) \triangleq \mathcal{D}_3(1+L_2)(1+L_1)(1+L),$$

$$L_2 \triangleq \frac{P_n \cdots P_2 G_2}{\mathcal{D}_3}$$

$$\frac{-X}{N_2} = \frac{G_2}{\mathcal{E}} = \frac{L_2/P_n \cdots P_2}{(1+L_2)(1+L_1)(1+L)} \qquad (11a\text{-}c)$$

$\doteq L_2/P_n \cdots P_2$ in the crucial hf. To minimize the latter it is best to let L_2 handle P_2 uncertainty only, leading to (cf (9a))

$$P_e^2 \triangleq \frac{\lambda_1\lambda_2 P_{a0} P_b + P_c}{1+P_{no}G_n + \cdots + P_{no}\cdots P_{30}G_3 + P_{no}\cdots P_{30}P_2G_2 + P_{no}\cdots P_{30}P_2P_1G_1}$$

$$= \frac{(\lambda_1\lambda_2 P_{ao} P_b + P_c)}{\mathcal{D}_{30}[1+\lambda_2 L_{20} + \lambda_1\lambda_2 L_{10}(1+L_{20})]} \quad , \quad \lambda_2 \triangleq \frac{P_2}{P_{20}} \qquad (12a\text{-}c)$$

with

$$\mathcal{V}^2 = \mathcal{V}_{\{P_e^2\}} = \left\{ \frac{\lambda_1\lambda_2 a_a k_b + k_c}{1+\lambda_2 L_{20} + \lambda_1\lambda_2 L_{10}(1+L_{20})} \right\}$$

instead of the smaller uncertainty set $\mathcal{V}^1$ of (9c).

The next step is to the find $B_2(\omega)$, the bounds on $L_{20}^0 \equiv L_{20}$, so that L_0, L_{10} designed for $\mathcal{V}^1$, remain satisfactory for $\mathcal{V}^2$. The resulting $B_2(\omega)$ are similar to $B_1(\omega)$: upper bounds in $I_{1A} = [0,\omega_{1x})$, lower ones in I_{1B} and closed curves merging into a B_{2H} etc. of length $\left(\frac{b_2}{a_2}\right)_{db}$ - see Fig. 7. The explanation is given in Appendix 2.

One can continue indefinitely in this manner. The resulting L_{20} (Fig. 4,7) has three intervals I_{2A}, I_{2B}, I_{2C} which decisively influence the bounds on a L_{30} designed to handle P_3 uncertainty, etc. The general forms for the $\mathcal{D}_i$, L_i, etc. are for $i = 1,\ldots,n$

$$\mathcal{D}_i = \mathcal{D}_{i+1}(1+L_i), \quad L_i = \frac{P_n \ldots P_i G_i}{\mathcal{D}_{i+1}}$$

$$\frac{-X}{N_i} = \frac{L_i/P_n \ldots P_i}{(1+L_i)(1+L_{i-1})\ldots(1+L)} \qquad (13a\text{-}d)$$

$$P_e^i = \frac{(\lambda_1\lambda_2 \ldots \lambda_i P_{ao} P_b + P_c)}{\mathcal{D}_{i+1,0}[1+\lambda_i L_{i0}+\lambda_i\lambda_{i-1}L_{i-1,0}(1+L_{i0})+\ldots+\lambda_i\ldots\lambda_1 L_{10}(1+L_{20})\ldots(1+L_{i0})]}$$

Note that F in Fig. 1a is available from Eq. 3e as soon as L_0 is known, by associating a nominal $T_0(s)$ with the nominal $L_0(s)$. But G_i is not known until $L_n, L_{n-1} \ldots, L_i$ are known. Thus from (13b)

$$G_n = \frac{L_{no}\mathcal{D}_{n+1,0}}{P_{no}} = L_{no}/P_{no}, \quad G_{n-1} = L_{n-1,0}\mathcal{D}_{n0}/P_{no}P_{n-1,0}$$

with $\mathcal{D}_{no} = 1 + L_{n0}$, etc.

Generality of structure. In the system considered, input R in Fig. 1 and $n+1$ plant outputs are available for processing, permitting an infinitude of $n+2$ degree of freedom structures [11]. The $n+2$ fundamental system functions are the system transfer function $T(s) = C/R$ and the $n+1$ loops $L, L_1, \ldots, L_n$. In any acceptable structure, L is gotten by cutting the outer loop just after the C sensor, giving in Fig. 1b, $L = PQHH_1H_2/\mathcal{D}_1$, $\mathcal{D}_1 = 1 + P_2H_2 + P_1P_2H_1H_2$. Keeping the first cut and with another cut after the C_1 sensor, gives $L_1 = P_2P_1H_1H_2/\mathcal{D}_2$, $\mathcal{D}_2 = 1 + P_2H_2$. $T(s)$ is always of the form $T = \psi L/(1+L)$, ψ independent of P_i, $\psi = 1/H$ in Fig. 1b. The design technique provides T and the nominal L_{i0} from which the compensations G_i (of Fig. 1a) or H_i (of Fig. 1b) or those of any other structure are derived. The excess of poles over zeros assigned to $T(s)$ e_T, must be compatible with the structure. In Fig. 1a, $e_T = e_F + e_L = e_F + e_P + e_G$ each a positive integer but in Fig. 1b, $e_L = \Sigma e_i = e_T + e_H$, $i = Q, H_1, H_2, P, H$.

IV PRACTICAL DESIGN PROCEDURE AND TRADE OFFS

Sections II, III described a design procedure based on the best (most economical) L_n, subject to the best L_{n-1}, ... , subject to the best L_1, in turn to the best L; first preference is given to L, then L_1, etc. This section shows how II, III provide the perspective for making reasonable trade-offs between the loops early in the game, without a detailed design. The display in Fig. 4 is used. The first step is an approximate single-loop L_S design. The low frequency bounds $B_S(\omega)$ based on P of (3b) are used which are hardly different from those based on P_e^0 of (7a) - see Sec. V. There is no need for a detailed design of L_{S0} for $\omega > \omega_{ds}$, at which L_{S0} reaches B_{HS} (analogs of ω_d, B_H in Fig. 3). Thus, the slope of L_{S0} is known on B_{HS} and the length of B_{HS} is that of the hf uncertainty of P. The slope of L_{S0} for $\omega > \omega_{xS}$ (analog of ω_x) is the same as of L_0 for $\omega > \omega_x$ -(cf L_0, L_{S0} in Fig. 4). Having L_{S0}, the approximate L_0 is immediately available because B_H is known (39.4 db shorter than B_{HS}).

Next, sketch an approximate L_{10} as follows. $|L_{10}|_{max}$ is near ω_z and its approximately value is obtained by the method of Appendix 1, Fig. A1b. The shape of $|L_{10}|$ for $\omega > \omega_{1z}$ is fairly standard. Its slope is $\approx$ -30 db/decade from ω_z to ω_{1x} in Fig. 4 until $|L_{10}(j\omega)| = 20 \log a_1/b_1 - \Delta$ db is attained (Δ a small gain margin), after which it is ~ constant for 1 - 1.5 octaves (ω_{1x} to Q_3), followed by a slope of $-20\, e_{L1}$ db/decade, with e_{L1} the chosen excess of L_{10} poles over zeros. Analogous to L_{S0}, L_{10}^* (Fig. 4) is L_{10} coping with all of P_a uncertainty. Similarly, an approximate L_{20} is obtained. $|L_{20}|_{max}$ is between ω_{1x} and Q_3 (Fig. 4) and its value can be found from Appendix 2. For $\omega > Q_3$, its shape is similar to that of $|L_{10}|$ for $\omega > \omega_z$. For

$n > 2$, the procedure is continued with $|L_{30}|_{max}$ near ω_{2x} , etc.

The next step is to sketch (Fig. 4) $|P_o|$, $|P_{10}\ldots P_{no}|$, $|P_{20}\ldots P_{n0}|$, $|P_{n0}|$. The noise amplifications in hf (3f, 13) are $|L_{S0}/P_0|$, $|L_0/P_0|$, $|L_{10}/P_{a0}|$, ... , $|L_{n0}/P_{n0}|$ for $|X/N|_S$, $|X/N|$, $|X/N_1|$, ... $|X/N_n|$ respectively, easily obtained by subtraction of the db values. The sensor noise effect $|X_i|$ is gotten by multiplying $|X/N_i|$ by $|N_i|$.

Trade-offs between the L_i are now considered, e.g., L_0 vs. L_{10} . L_0 of II is one extreme, L_{S0} is the other and intermediate designs are possible. One poorer by $\alpha = 5$ db is shown in Fig. 3, postponing the $J_1J_2J_3$ pattern in Fig. 4 until $|L_0|$ is less by 5 more db with $(\omega_z)_{new} > (\omega_z)_{old}$. In return, the peak of the new $|L_{10}|$ (Appendix 1, Fig. A1b) is $\approx$ -18.5 instead of -9db. Trade-off between L_0 and L_1 is made with no reference to L_2, L_3,.... Trade-off between L_{10} and L_{20} is done in the same manner etc.

Bandwidth Propagation and Similarity with the Cascade Plant structure

Let the bandwidth $BW(L_i)$ be arbitrarily defined as that at which $|L_{i0}|$ achieves its final asymptotic slope: ω_z for L_0, Q_3 for L_{10}, X_2 for L_{20} in Fig. 4. $BW(L_i)$ increases with i. This phenomenon occurs in precisely the same manner in the cascade-system [10]. The relations between the L_{io}, the role of b_i/a_i, the sensor noise effects and trade-offs etc. are very similar in the two structures. However, the values of $|L_{i0}|_{max}$ are different and the derivation is more difficult here. Here, at each new L_i stage, one must use a more complex form of P_e. In the cascade system the step from i to i + 1 is identical the that from i - 1 to i. But the final results are remarkably similar.

In Fig. 4, $BW(L_{no}) = X_2$ is comparable with $BW(L_{S0})$ at X_0, a little larger due to the extra few db of gain margin needed per section.

Thus, the final cut-off frequency for a single-loop design is comparable to that for a multiple-loop design, but they are associated with different loops so there can be a great improvement in sensor noise effect. Thus, in Fig. 4, $(X_2-X_0)_{db} = -22 + 91 = 69$ db, while $|P_{20}|_{db} - |P_0|_{db} = 127$ db, an improvement if $|N_2/N| < 127-69 = 58$ db. In practice it is reasonable to assume that the plant power levels and with them the sensor noise levels increase in proceding from input to output. The design procedure is highly transparent permitting a good estimate of the optimum division between the feedback loops, without a detailed design.

High-frequency uncertainty

Clearly, multiple-loop design can be highly superior to single-loop, for large hf plant uncertainty. The linearized plant model is usually due to linearization of a nonlinear plant about an operating point or trajectory. Large variations can exist due to different operating points, e.g. in flight control [17], where values > 1000 have been reported.

It has been proven that in a large class of linear and nonlinear time-varying uncertain plants the latter can be represented for synthesis purposes by an equivalent linear time-invariant uncertain plant set $P_{eq}[s]$ [12, 13]. The set equivalence is exact with respect to a prescribed acceptable plant output set. Linear time invariant design applied to the $P_{eq}[s]$ problem is guaranteed to work for the original nonlinear problem. A nonlinear plant with no uncertainty can thus generate large hf uncertainty in $P_{eq}[s]$, e.g. consider $y = k^3x^3$, x the input and y the output. Suppose fairly linear response is desired for $y = A^3(1-e^{-t})^3$, $A \in [0.5,5]$. To find $P_{eq}[s]$, evaluate $\frac{Y(s)}{X(s)} = P_{eq} = \frac{6kA^2}{(s+2)(s+3)}$ in this case. Since $A \in [0.5,5]$, the hf gain of P_{eq} varies by a factor of 100, due to A^2. For a simple dynamic example, consider $\dot{y} + By^{1/3} \operatorname{sgn} y = kx$, giving

$P_{eq} = \dfrac{6kA^3}{(s+3)[BAs+6A^3+2BA]} \to 6kA^2/Bs^2$ at hf, with uncertainty factor of 100.

V. JUSTIFICATION OF ASSUMPTIONS

General plants. This section is devoted to the justification of simplifying assumptions in II, III. One was use of $P_i = k_i/s^{e_i}$ for all ω, not just in hf where it is applicable. Recall in Sec. II the first step was to find the smallest $\{P_e^0\}$ of (6a), by minimizing over $G_1,\ldots,G_n$ and the values of $P_{10},\ldots,P_{n0}$. Suppose $P_j = k_j/(s+q_j)$ with k_j, q_j uncertain. This minimization problem is extremely difficult at medium ω. Fortunately it makes little difference if it is not done at all. The reason is that which made L_{10} unnecessary in I_A, L_{20} in I_{1A} etc., i.e. under certain conditions there is little difference in $|L_0=GP_0|_{min.}$ needed, whether $\{P\}$ = set S_1 or set $S_2 \ll S_1$. In Fig. 3, suppose that instead of AB (A at X_2), the uncertainty set is ABEFG with E,F extending even to ∞. L_0 at X_2 results in almost the same $\Delta\ell n|T|$ for both (23.85 db instead of 23.5db).

It is therefore concluded that in most of I_A, $\{P\}$ of (3b) be used for L_0 design, just as in L_S design. P_e^0 is used only for ω where P_j is well approximated by k_j/s^{e_j}. This has been verified for several numerical examples; e.g. for $n = 1$ with $P_a = k/(s+q_a)$, $P_b = k_b/s$ $P_c = k_c/s(s+q_c)$, $k_a \in[1,400]$ $k_b \in[1,60]$, $k_c \in[1,200]$, $q_i \in[0.5,2]$, all independently uncertain. The maximum difference in the two $B(\omega)$ is only three db even though the difference between $\{P\}$ and $\{P_e^0\}$ is $\approx$ 40db. If this conclusion is incorrect for an unusual case, then it is also likely that the obligations on L_{10} in I_A will be greater too. By using $\{P\}$ in medium ω, one is certain that the obligations on L_{10}

in I_A will be negligible, as in Sec. II. The simple and transparent forecasting of Sec. IV may then be used. If these indicate less than desired saving in sensor noise effect, then one can return to check if greater saving is possible with P_e^0 in I_A.

Another assumption in II was $b_c/a_c > b_b/a_b$. If the opposite is true then minimum Lgth $\{P_e^0\}$ is at $k_a = b_a$ of value $(b_a b_b + b_c)/(b_a a_b + a_c)$. There exist a set of g_i which achieve this and the procedure is precisely the same as before. A third assumption is that $e_a + e_b = e_c$ giving (4) with $\{P_e\}$ in hf a vertical line in the Nichols chart. If $|e_a + e_b - e_c| \triangleq \delta \neq 0$ is even, the result is also a vertical line whose length is a function of ω. The design procedure is basically the same. It is possible that $P(j\omega) = 0$ at finite $\omega = \omega_1$ at some combinations of parameters, giving $T(j\omega_1) = 0$. If so, the specifications on $T(j\omega)$ and $C/D(j\omega)$ must allow for this. If δ is odd, design is more complicated because min. Lgth $\{P_e^0\}$ does not necessarily exist. The range of $\{P_e^0\}_a$ (i.e., at any fixed P_a value) is no longer a line but a two-dimensional region and there may not exist a set of g_i values in (4a) such that the resulting $\bigcup_a \{P_e^0\}_a$ fits into any one $\{P_e^0\}_a$. It is then a matter of judgment how to exploit the available freedom to optimize L_0. This case has not been studied in detail. However, the design technique of secs. II, III provides the understanding for good use of the design variables. One knows the kinds of distortions of the uncertainty set which are useful in relation to I_A, I_B, etc.

Another assumption was that the disturbance attenuation was a minor problem, dealt with by (2,10). The procedure is basically the same if it is a major problem, for then $C_D = C/D$ must satisfy $|C_D(j\omega)| \leq \gamma(\omega)$ over $\{P\}$. This can be translated [15] into bounds $B_D(\omega)$ on $L_0(j\omega)$. The

more stringent of $B_D(\omega)$ and of $B(\omega)$ due to (1), is used but thereafter the design procedure is the same.

Unstable and Nonminimum-phase plants. Open-loop stable minimum-phase plants were assumed in II, III for simplicity. But clearly the design procedure applies so long as the L_{i0} exist which satisfy the $B_i(\omega)$. Consider L_0 first. It must handle $\{P_e^0\}$ giving (Sec. II) a single-loop problem. The latter is solvable if $\{P_e^0\}$ contains open-loop poles whose range of uncertainty includes part of the right-half as well as the left-half plane [15,18]. If however, $\{P_e^0\}$ includes nonminimum-phase elements then L_0 exists only if the performance specifications are compatible with the now limited bandwidth [18] of L_0.

The same conclusions apply to the inner loops. Again, right half-plane P_i poles pose no problem, but such zeros impose limitations on L_{i0}.

VI. CONCLUSIONS

For a class of feedback systems with large uncertainty, a multiple-loop design results in sensor noise sensitivity much smaller than in a single-loop design satisfying the same specifications. The designer can divide up the feedback burden among the loops in a sensibly optimum manner, wherein the uncertainties of the plant sections, their levels and associated sensor noise sources play important roles. An important feature of the design techniques is its transparency. In return for learning the mechanics of sensitivity reduction in the language of frequency response, there is gained excellent insight into the trade-offs between the loops and the overall cost of design in terms of bandwidth and noise sensitivity - even without performing the detailed design.

It is discouraging that we must at this time separately develop a design technique for each different structure. However, it is encouraging that although the present derivation is much more difficult than for the cascade system, the results are remarkably similar. This leads to the expectation of similar results for any multiple-loop single input-output structure. It is probably necessary to extend quantitative design to some additional complex structures before the general pattern will become clear for any multiple loop, single input-output plant.

APPENDIX I - BOUNDS $B_1(\omega)$ ON FIRST INNER LOOP

Sec. III presented without explanation the bounds $B_1(\omega)$ in terms of the intervals I_A, I_B, I_C of $L_0(j\omega)$. The explanation is available by considering the uncertainty or variation set (9c)

$$\mathcal{V}^1 = \left\{ \frac{\lambda_1 a_a k_b + k_c}{1 + \lambda_1 L_{10}} \right\} \supset \mathcal{V}^0 = \{a_a k_b + k_c\} \text{ of (5a).}$$

$\mathcal{V}^0$ is the line AB in Figs. A1a-c, whereas $\mathcal{V}^1$ is the larger set ABC_jD_j, a function of L_{10} and λ_{1max}. The point A is always the nominal L_0, $\lambda_1 = 1$, $k_b = a_b$, $k_c = a_c$ irrespective of the value of L_{10}, because that is the objective of the $B_1(\omega)$. Attention is focused on the range $-\pi < \text{Arg } L_{10} < 0$. The following properties of $\mathcal{V}^1$ are important.

(P1) In Fig. A1a, as $|L_{10}|$ is increased at fixed Arg L_{10}, boundaries BC_i, BD_i shift downward - compare BC_3C_3' at 0 db with BC_2C_2' at -20 db and BC_1C_1' at -40 db; and similarly the BD_iD_i'.

(P2) For fixed L_{10}, the effect of increase in λ_1 is extension of the BC_i, AD_i, i.e., widening of the regions by decreasing amounts, to a maximum of

$$\left|\theta - \tan^{-1} \frac{m\sin\theta}{1+m\cos\theta}\right|$$

at $\lambda_1 = \infty$, where $L_{10} = m \angle\theta$. This effect of large λ_1 is important in explaining the nature of $B_2(\omega)$.

(P3) For given λ_{1max} and $|L_{10}|$, $\mathcal{V}^1$ at $\angle L_{10} = \theta$ is the mirror image (about AB) of $\mathcal{V}^1$ at $\angle L_{10} = -\theta$.

The upper bounds of $B_1(\omega)$ in I_A are explained by property (P1) in

Fig. Ala. A family of $\mathcal{V}^1$ at fixed $\angle L_{10} = -90°$ is tried at $\omega = 40 \in I_A$ i.e., point A of $\mathcal{V}^1$ is set at $L_0(j40) \doteq -32$ db $\angle -130°$ (from Fig. 3) at which Fig. 1 requires

$$\Delta\left|\frac{T_{max}}{T_{min}}\right| \leq 34.3 \text{ db} \quad .$$

At $\omega = 40$ (1), (2) are precisely satisfied. It is seen in Fig. Ala that at Arg $L_{10} = -90°$, $|L_{10}| < -20$ db is OK while $|L_{10}| \geq 0$ db is not because $\Delta|T| = |-34-2.3| = 36.3$ db and larger $|L_{10}|$ gives larger $\Delta|T|$. The upper bound here is between 0 db and -20 db. From a study of the shape of constant $|L/1+L|$ loci on the Nichols chart, it is seen that this result applies for all $\omega \in I_A$ at which Arg $L_0 \leq -90°$. In Fig. 3, there is a small interval in which Arg $L_0 > -90°$ and in general there may be a low frequency region where Arg $L_0 > -90°$. However, the final result is basically the same, because of the very small sensitivity of the loci of constant $|L/1+L|$ on the Nichols chart at large $|L|$.

It is worth noting that if L_{10} did not exist at all, then $\mathcal{V}^i$ $i = 1, \ldots n$ would only be a much longer vertical line with lowest point at A. From Fig. Ala, both (1) and (2) would still be satisfied. Thus for $\omega \in I_A$, L_0 designed for P_B, P_C uncertainty only, automatically handles $P_1 \ldots P_n$ uncertainty as well. However L_1 is needed in I_B, precluding $L_{10} \equiv 0$ in I_A and giving there upper bounds as in Fig. Ala. Similarly note that in I_A, $B_1(\omega)$ are hardly affected by large increase of λ_1 - see Fig. Ala. Therefore L_{10} could handle the entire uncertainty of P_a i.e. λ_a in place of λ_1 if $G_2 = G_3 = \ldots G_n = 0$.

Property (P1) also explains in Fig. A1b the lower bounds in l_B. At $|L_{10}| = m_1$, $\mathcal{V}^1$ penetrates into M < 2.3 db, violating (2). Thus in Fig. A1b, at Arg $L_{10} = \theta$, $|L_{10}|_{min} = m_2$. In this range, (2) easily dominates so there is no danger of violating (1) (cf Fig. A1a) except possibly at very large $|L_{10}|$, which would not be used anyhow. Here too, λ_1 could be increased to ∞ without affecting $B_1(\omega)$ - recall (P2), the effect of large λ_1 on $\mathcal{V}^1$ in Fig. A1a and the critical factors in Fig. A1b. Thus there is no need for $L_2,\ldots L_n$ in l_B as well. (P1) also explains in Fig. A1c the upper and lower bounds in l_C. Thus, at $\angle L_{10} = \theta$, $|L_{10}|$ must be either $< m_2$ or $> m_5$. From (P2) the width of $\mathcal{V}^1$ is $< |\text{Arg } L_{10}|$. Hence, Fig. A1c shows that as ω increases in l_C, the value of $-\text{Arg } L_{10}$ for which all $|L_{10}|$ are acceptable, increases steadily, explaining why the $B_1(\omega)$ closed curves shrink to B_{1H} in Fig. 6b. B_{1H} length is $\left(\frac{b_1}{a_1}\right)_{db}$ because at Arg $L_{10} = -\pi$ (say at $\omega_{1\pi} \simeq 1{,}000$ here) $1 + \lambda_1 L_{10} = 1 - \lambda_1 |L_{10}|$ with $|L_{10}| < 1/\lambda_{1max} = \frac{a_1}{b_1}$; otherwise $\mathcal{V}^1$ extends in length to ∞ and being 360° wide, must intersect with the forbidden $\left|\frac{L}{1+L}\right| < \gamma = 2.3$ db regions located at Arg $L = \pm n\pi$, $n = 1,3,\ldots$ This is also seen from (10), for let $L_i = \lambda_i L_{io}$, and $P_\alpha = P_{\alpha o}$ for $a \neq i$. Then at Arg $L_{io} = -\pi$, $|L_{io}| < 1/\lambda_{imax}$ is essential, otherwise $|C_i/D_i|$ is infinite at λ_{imax}.

Increase of λ_1 affects the bounds at m_2, requiring $|L_{10}| < \beta m_2$, $\beta < 1$, but not the lower boundary at m_5. In Fig. 6b it is seen that L_{10} lies on the upper part of $B_1(\omega)$ for most of l_{1A}, so L_{10} designed to handle P_1 only, can also cope with $P_2,\ldots,P_n$ if $L_2 \equiv \ldots \equiv L_n \equiv 0$.

APPENDIX 2 - BOUNDS ON SECOND AND HIGHER INNER LOOPS

The function of L_{20} is to guarantee that L_{10} is satisfactory despite its design on the basis of P_e^1 of (9a). It was seen in Appendix 1 that for $\omega \in I_A$, I_B and part of I_C, L_{10} suffices i.e. L_{20} may be zero. This is so only for $\omega < \omega_{1\pi}$ at which $\angle L_{10} = -\pi$. It was noted also that $|L_{10}(j\omega_{1\pi})| < \frac{1}{\lambda_{1max}}$, so L_2 is needed for $\omega = \omega_{1\pi}$.

Hence, $L_{20} \equiv 0$ is impossible in I_{1A} and it is not surprising that the $B_2(\omega)$ there are upper bounds (recall in Appendix 1 precisely the same situation for $L_{10}(j\omega)$ in I_A). At $\omega = \omega_{1\pi} \in I_{1B}$, $1+\lambda_{1max}L_{10} = \epsilon > 0$ (.38 in the example), so the denominator (12a) of P_e^2 is $\mathcal{D}_{30}(1-\lambda_2+\epsilon\lambda_2+\epsilon\lambda_2 L_{20})$, and for it $\neq 0$ at Arg $L_{20}=0$, $|L_{20}| > \frac{1-\epsilon}{\epsilon} - \frac{1}{\epsilon\lambda_{2max}}$ = 1.4 here. So there is a lower bound on $|L_{20}(j\omega_{1\pi})|$ which is a function of Arg L_{20}.

To find $B_2(\omega)$ in I_{1C} it is necessary to use P_e^2 of (12a) in place of P_e^1 of (9a). It is convenient, however, to express P_e^2 in terms of P_e^{1*}, defined as P_e^1 with $\lambda_1\lambda_2$ replacing λ_1, because $\mathcal{V}\{P_e^2\}$ is easier expressed in terms of $\mathcal{V}\{P_e^{1*}\}$, while $\mathcal{V}\{P_e^{1*}\}$ is easily gotten from $\mathcal{V}\{P_e^1\}$ shown in Fig. Ala by letting $\lambda_1 > \lambda_{1max}$. From (12a) and replacing λ_1 in (9a) by $\lambda_1\lambda_2$,

$$\frac{P_e^2}{P_e^{1*}} = \frac{(1+\lambda_1\lambda_2 L_{10})}{\left(\frac{1+\lambda_2 L_{20}}{1+L_{20}}\right) + \lambda_1\lambda_2 L_{10}} = \frac{OV}{OC_i} \qquad \text{(A1)}$$

in Fig. A2, as follows. Let $OQ = \lambda_1\lambda_2 L_{10}$ (Arg $L_{10} < -\pi$ in I_{B1}, I_{C1}), $QV = 1$, $QD_i = a$, $|D_iV| = |aL_{20}|$, Arg E_iD_iV = Arg $E_iD_iC_i$ = Arg L_{20}, $D_iC_i = \lambda_2 D_iV = \lambda_2 aL_{20}$, so $OV = OQ + QV = \lambda_1\lambda_2 L_{10} + 1$,

$$QC_i = \frac{QC_i}{1} = \frac{QD_i + D_iC_i}{QD_i + D_iV} = \frac{a + a\lambda_2 L_{20}}{a + aL_{20}} = \frac{1 + \lambda_2 L_{20}}{1 + L_{20}} \text{ and}$$

$$OC_i = OQ + QC_i = \lambda_1\lambda_2 L_{10} + \frac{1 + \lambda_2 L_{20}}{1 + L_{20}}, \text{ giving (A1).}$$

Fig. A2 was sketched for $\omega = 2000$, $\lambda_1 = 40$, $\lambda_2 = 10$, at which (Fig. 6b) $L_{10} = .0158 \angle -230°$, $L_o = -127$ db $\angle -430°$, for assumed Arg $L_{20} = -117°$ constant. The D_i describe an arc of a circle as $|L_{20}|$ is varied, as do the C_i drawn for $\lambda_2 = 10 = \lambda_2$ max, i.e. $D_iC_i = 10\ D_iV$. Clearly for $|L_{20}| << 1$, $OV/OC \to 1$ and for $|L_{20}| >> 1$, $|OV/OC| < 1$, so such $|L_{20}|$ are acceptable. Obviously $\exists\ \lambda_2 < \lambda_{2max}$, $\ni$ resulting C_i circle passes through 0, giving infinite OV/OC_i and the resulting $\mathcal{V}\{P_e^2\}$ passes thru M = 2.3 db. Thus, $\exists$ upper and lower bounds in this ω range. As ω increases, $|L_{10}|$ and its angle drecrease, so the arc $C_iC_j\ldots$ does not extend to 0 in Fig. A2 and any $|L_{20}|$ is acceptable. Hence, the $B_2(\omega)$ tend to a line B_{2H} at $-\pi$, from 0 to $(a_2/b_2)_{db}$. $B_2(\omega)$ are shown in Fig. 7, including a sensibly optimum $L_{20}(j\omega)$ with its intervals I_{2A}, I_{2B}, I_{2C}.

For the third inner loop (if $n > 2$), $P_{\hat{e}}^3$ is needed and there is an analogous situation with respect to I_{2A}. At I_{2B}, $\omega_{2\pi}$ (at which Arg $L_{20} = -\pi$) is very large (~ 6500) and as before, there is a lower bound on L_{30} at $\omega_{2\pi}$. For $\omega \geq \omega_{2\pi}$, $|L_o|$, $|L_{10}| << 1$, so (in 13d), Denom. $(P_e^3) \to 1 + \lambda_3 L_{30} + \lambda_3\lambda_2 L_{20}(1 + L_{30})$, similar to Denom. (P_e^2) if i is replaced by i - 1. P_e^3/P_e^{2*} similar to (A1) is obtained giving a figure similar to Fig. A2 and analogous $B_3(\omega)$. The process is continued to $B_4(\omega)$, ..., $B_n(\omega)$.

REFERENCES

1. V. M. Popov: Hyperstability and optimality of automatic system with several control functions. Rev. Roum. Sci. Tech., Ser. Electrotech. Energ. 9, 629-690 (1964).

2. W. M. Wonham: On pole assignment in multi-input controllable systems. IEEE Trans. Aut. Control AC-12, 660-665 (1967).

3. I. Horowitz and U. Shaked: Superiority of transfer function over state-variable methods in linear time-invariant feedback system design. IEEE Trans. Aut. Control AC-20, 84-97 (1975).

4. D. G. Luenberger: Observers for multivariable systems. IEEE Trans. Aut. Control AC-11, 190-197 (1966).

5. J. D. Simon, S. K. Mitter: Synthesis of transfer function matrices with invariant zeros. IEEE Trans. Aut. Control AC-14, 420-421 (1969).

6. J. B. Pearson, R. W. Shields, P. W. Staats, Jr.: Robust solutions to linear multivariable control. Ibid AC-19, 508-517 (1974).

7. E. J. Davison: The robust control of a servimechanism problem for linear time-invariant multivariable system. Ibid AC-21, 25-34 (1976).

8. S. P. Bhattacharyya: The structure of robust observers. Ibid AC-21, 581-588 (1976).

9. M. G. Safonov, M. Athans: Gain and phase margins for multiloop LQG regulators. Ibid AC-22, 173-179 (1977).

10. I. Horowitz, M. Sidi: Synthesis of cascaded multipole-loop feedback systems with large plant parameter ignorance. Automatica 9, 589-600 (1973).

11. I. Horowitz: Synthesis of Feedback Systems. Academic Press, New York (1963).

12. I. Horowitz: A synthesis theory for linear time-varying feedback systems with plant uncertainty. IEEE Trans. Aut. Control AC-20, 454-464 (1975).

13. I. Horowitz: Synthesis of feedback systems with nonlinear time-varying uncertain plants to satisfy quantitative performance specifications. Proc. IEEE, 123-130 (1976).

14. H. W. Bode: Network Analysis and Feedback Amplifier Design. Van Nostrand, New York (1945).

15. I. Horowitz, M. Sidi: Synthesis of feedback systems with large plant ignorance for prescribed time domain tolerances. Int. J. Control 16, 287-309 (1972).

16. I. Horowitz: Optimum loop transfer function in single-loop minimum-phase feedback systems. Int. J. Control 18, 97-113 (1973).

17. M. A. Ostgaard, E. B. Stear, P. C. Gregory: The case for adaptive controls. Agard Flight Mechanics Tech. Report Sec. III, Paris, France, July 1962.

18. I. Horowitz, M. Sidi: Optimum synthesis of nonminimum-phase feedback systems with parameter uncertainty. Int. J. Control, to appear.

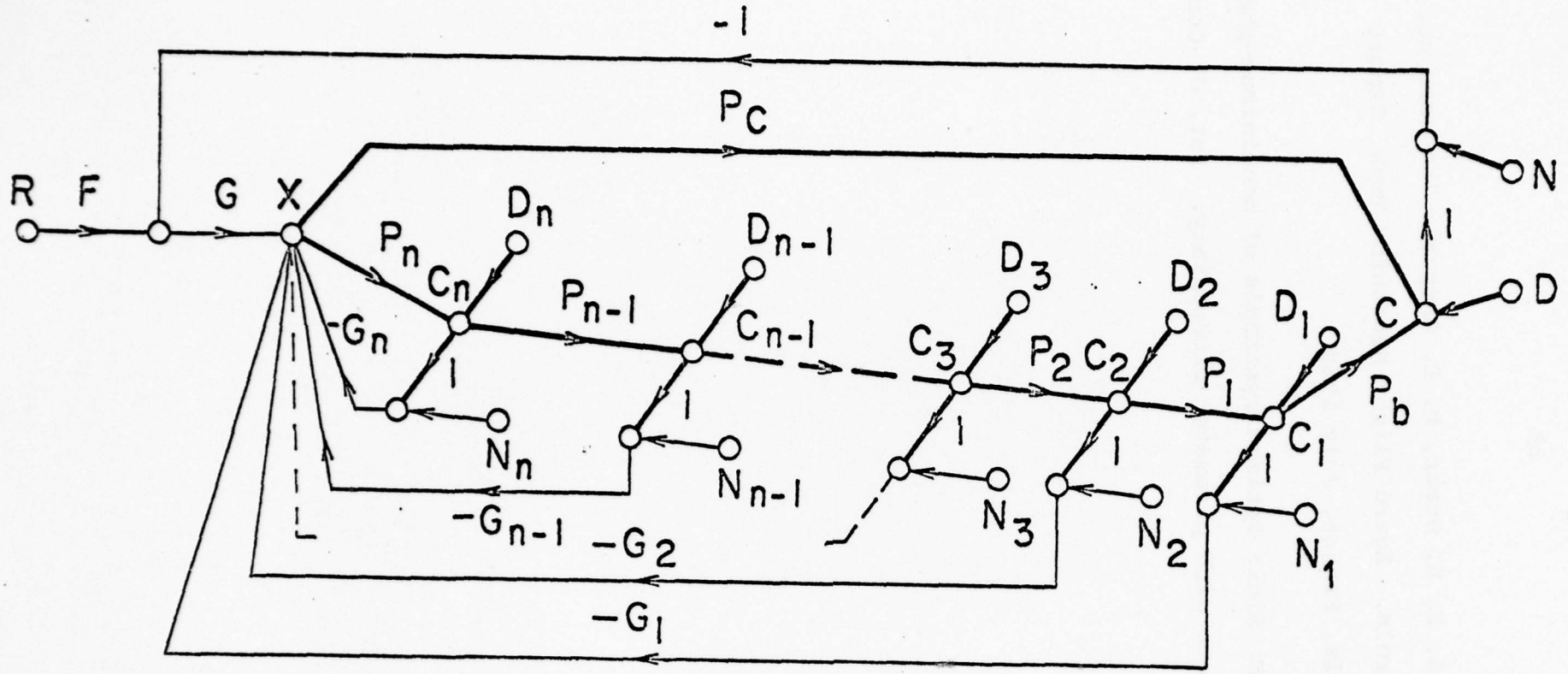

Fig. 1a Multiple-loop system with a n+2 degree of freedom structure. Darker lines indicate constrained plant, sensors, etc.

$$P_a = P_1 P_2 \cdots P_{n-1} P_n \qquad P = P_a P_b + P_c$$

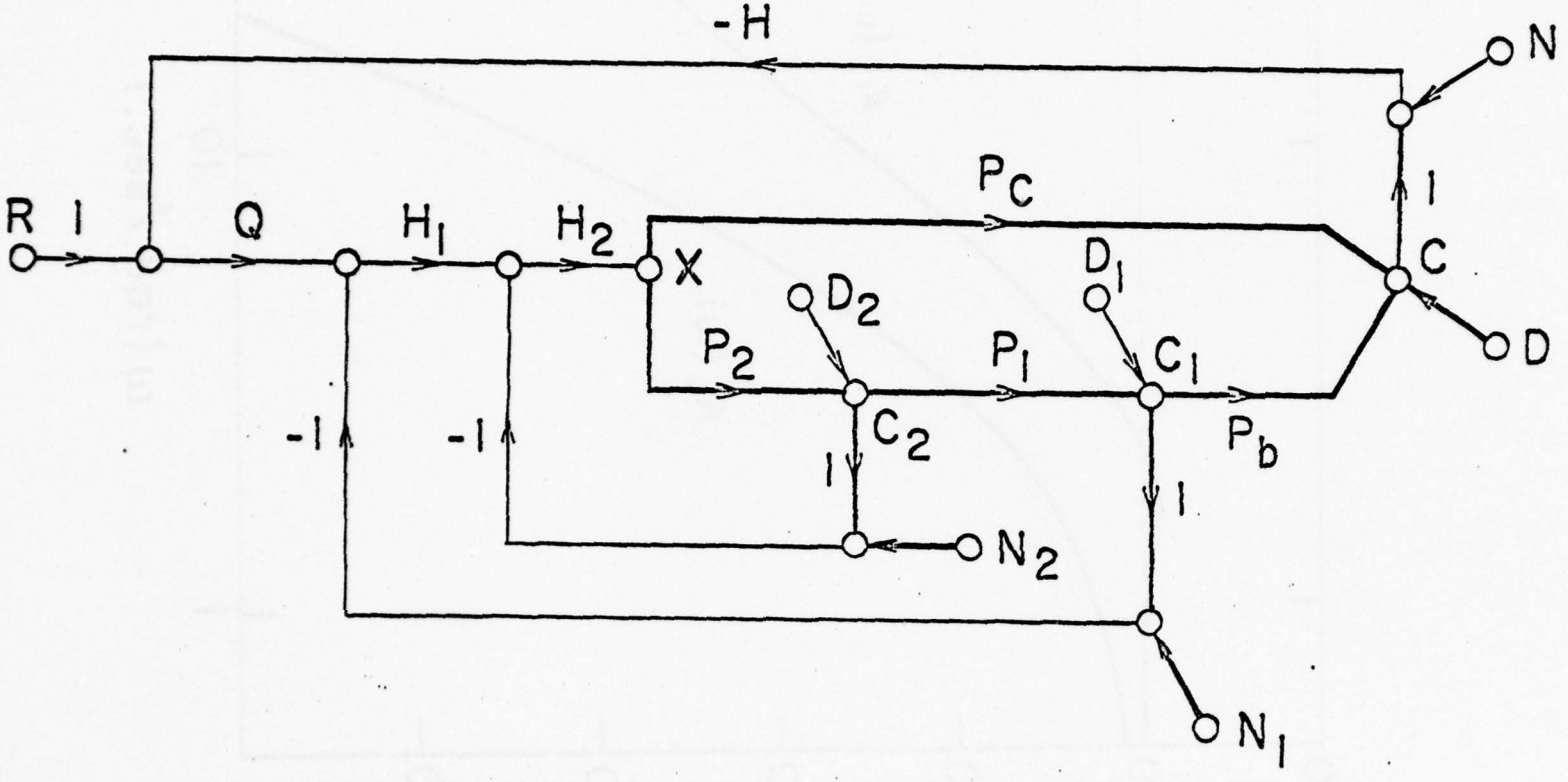

Fig. 1b Multiple-loop system for $n = 2$, with a different 4 degree of freedom structure.

$$P_a = P_1 P_2, \quad P = P_a P_b + P_c$$

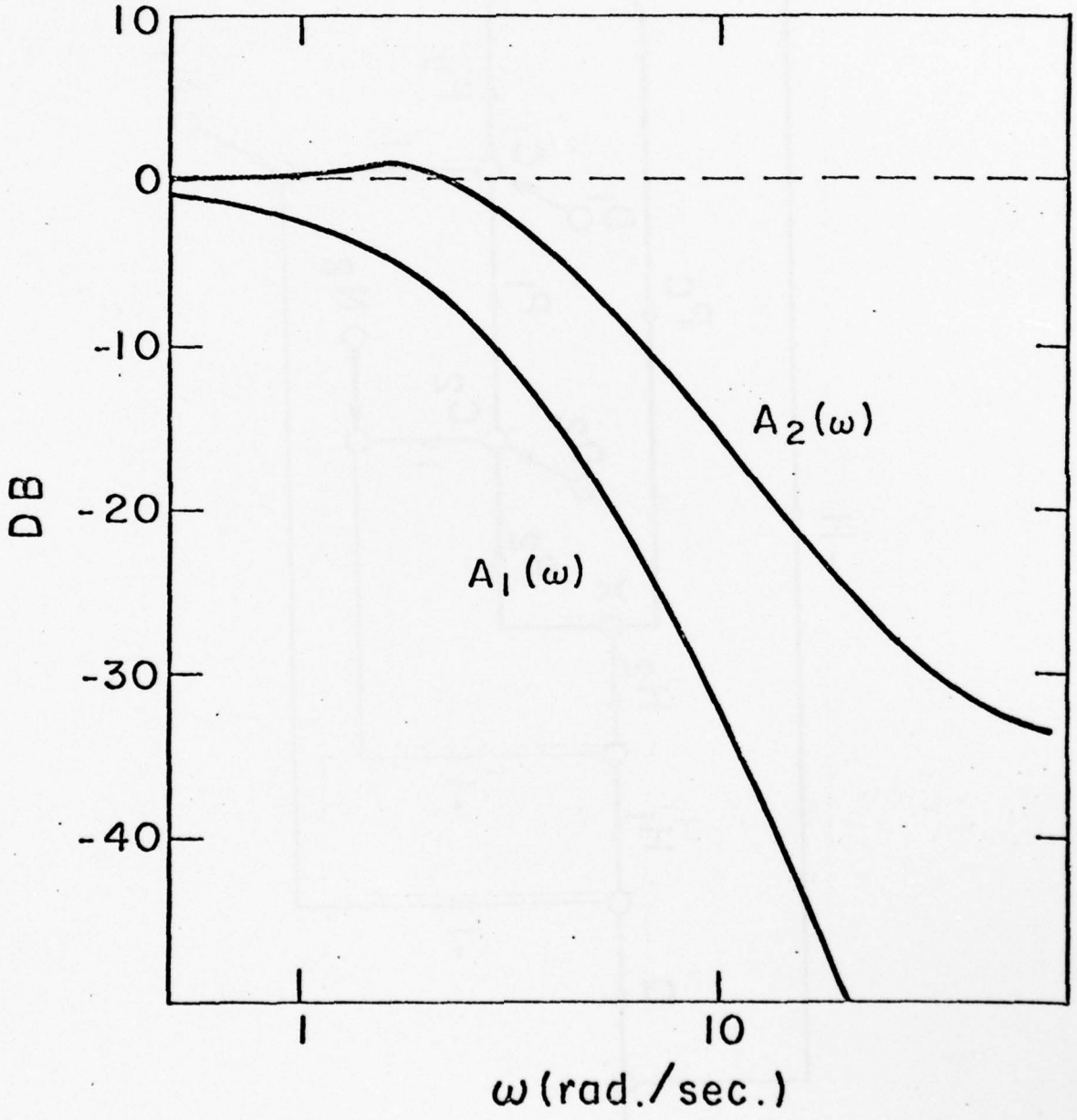

Fig. 2 Specified bounds on $|T(j\omega)|$.

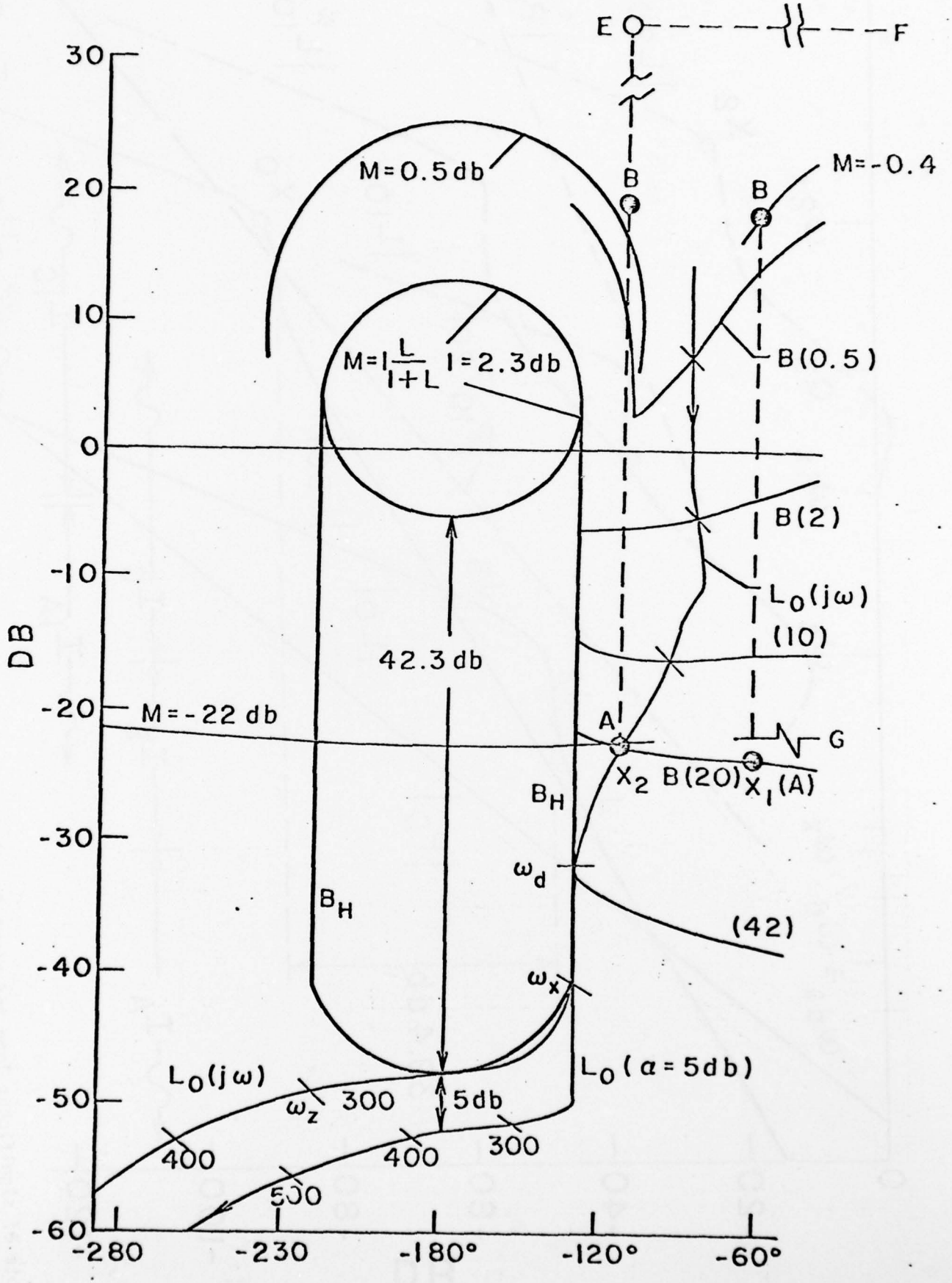

Fig. 3 Bounds B(ω) on $L_o(j\omega)$ in Nichols chart.

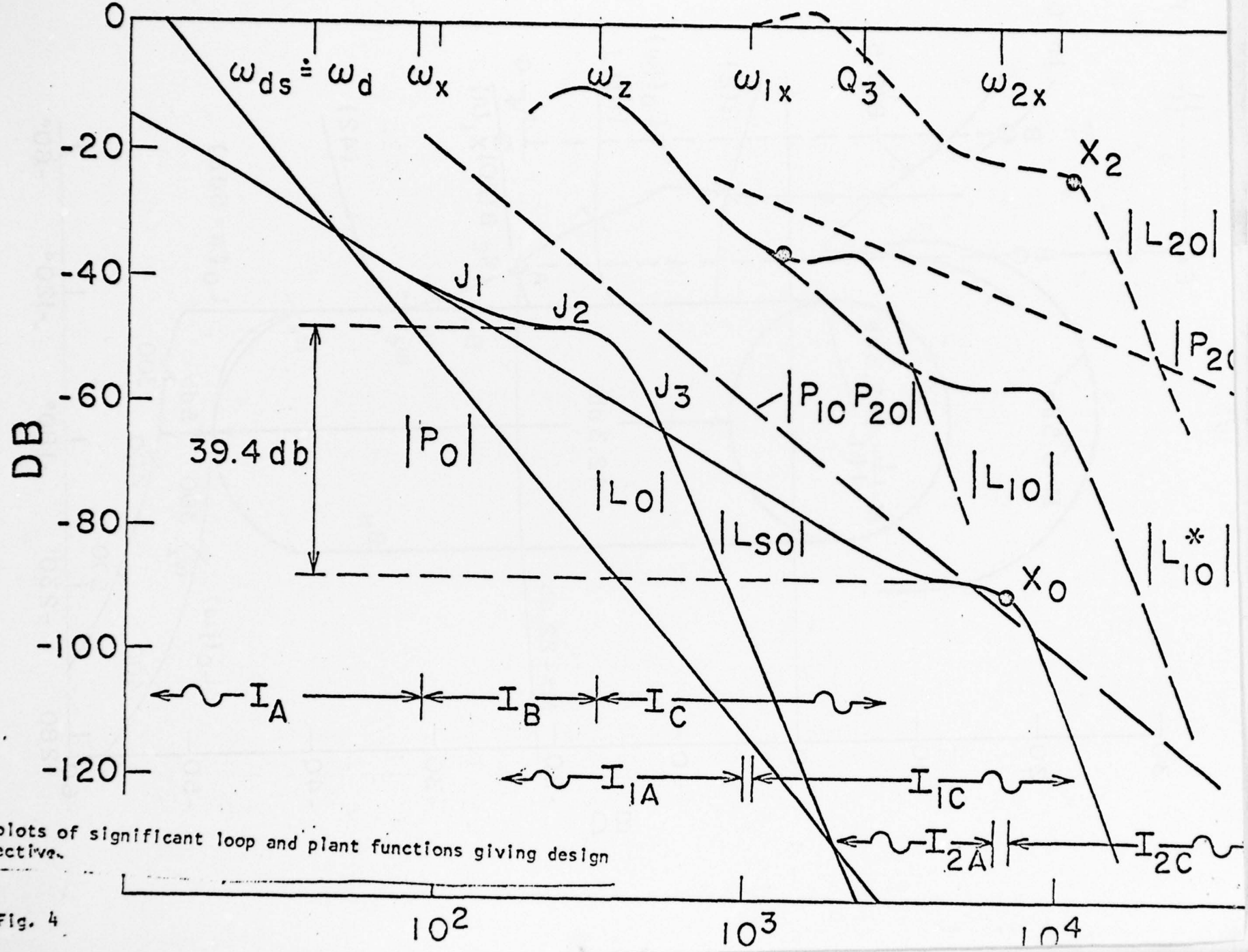

Bode plots of significant loop and plant functions giving design perspective.

Fig. 4

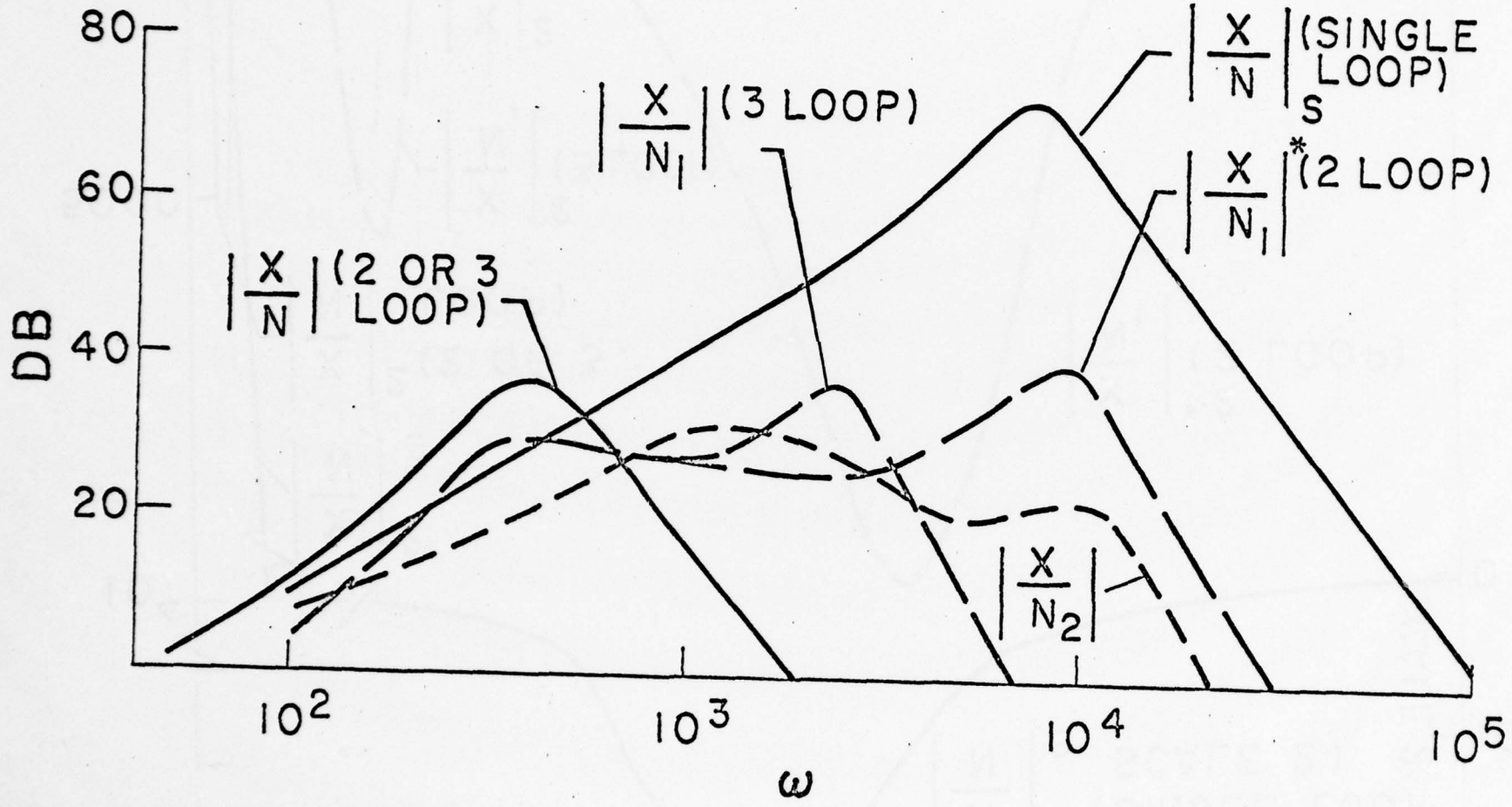

Fig. 5a Sensor noise effects at X or Pod

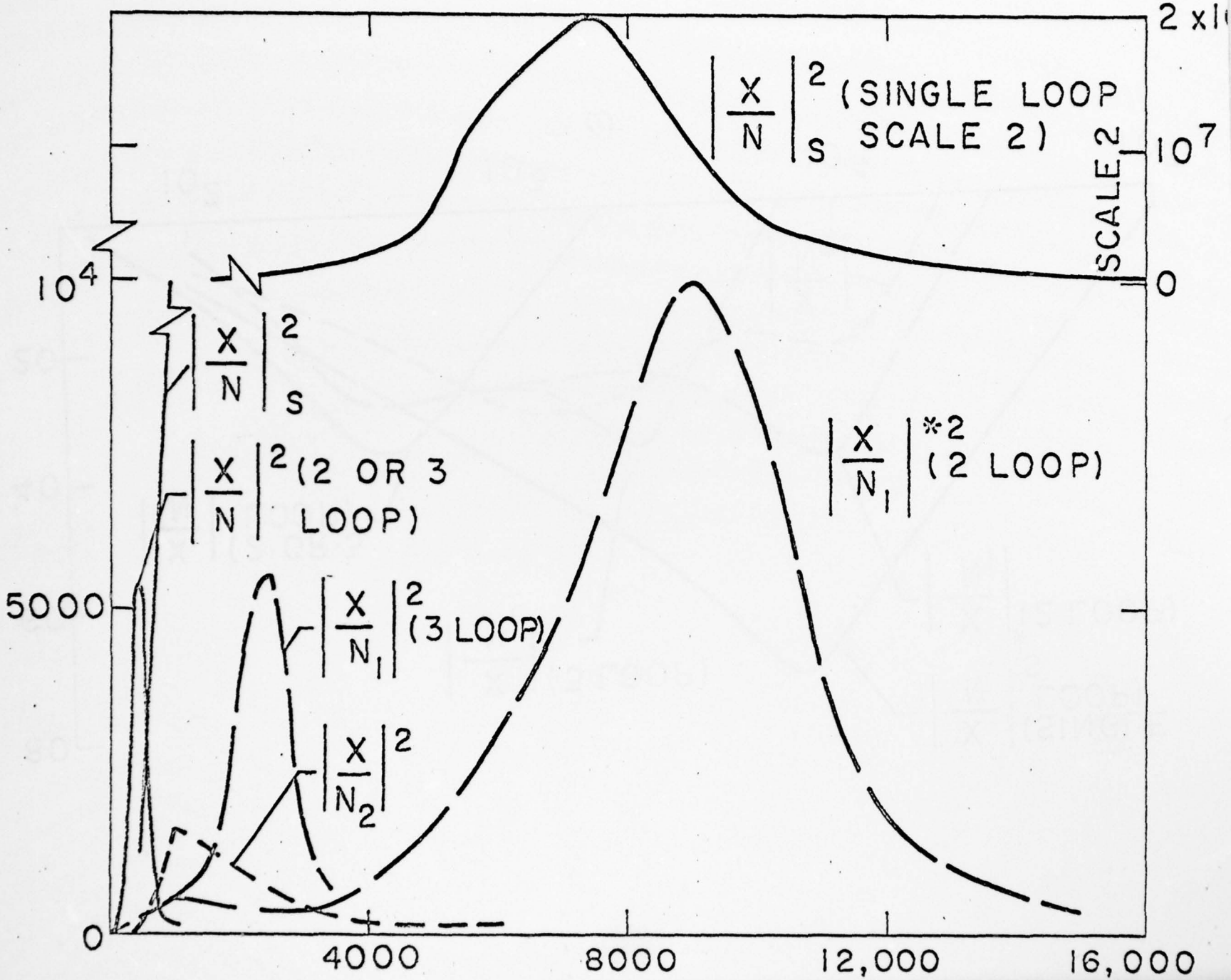
$\left|\frac{X}{N}\right|^2_S$ (SINGLE LOOP SCALE 2)
SCALE 2
2 x 1
10^7
0
10^4
$\left|\frac{X}{N}\right|^2_S$
$\left|\frac{X}{N}\right|^2$ (2 OR 3 LOOP)
$\left|\frac{X}{N_1}\right|^2$ (3 LOOP)
$\left|\frac{X}{N_2}\right|^2$
$\left|\frac{X}{N_1}\right|^{*2}$ (2 LOOP)
5000
0
4000
8000
12,000
16,000

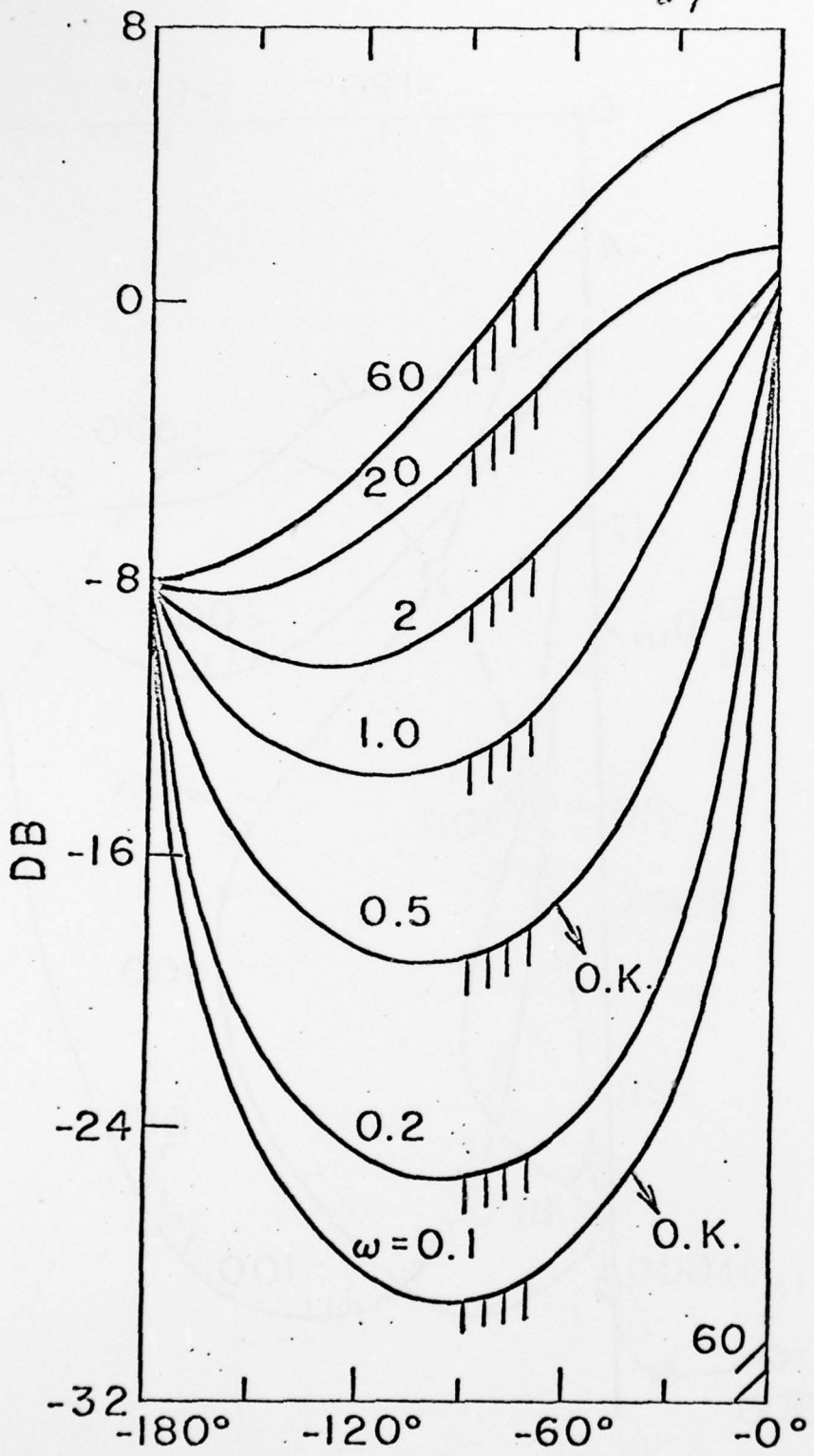

Fig. 6a Bounds $B_1(\omega)$ on $L_{10}(j\omega)$ in I_A are upper bounds.

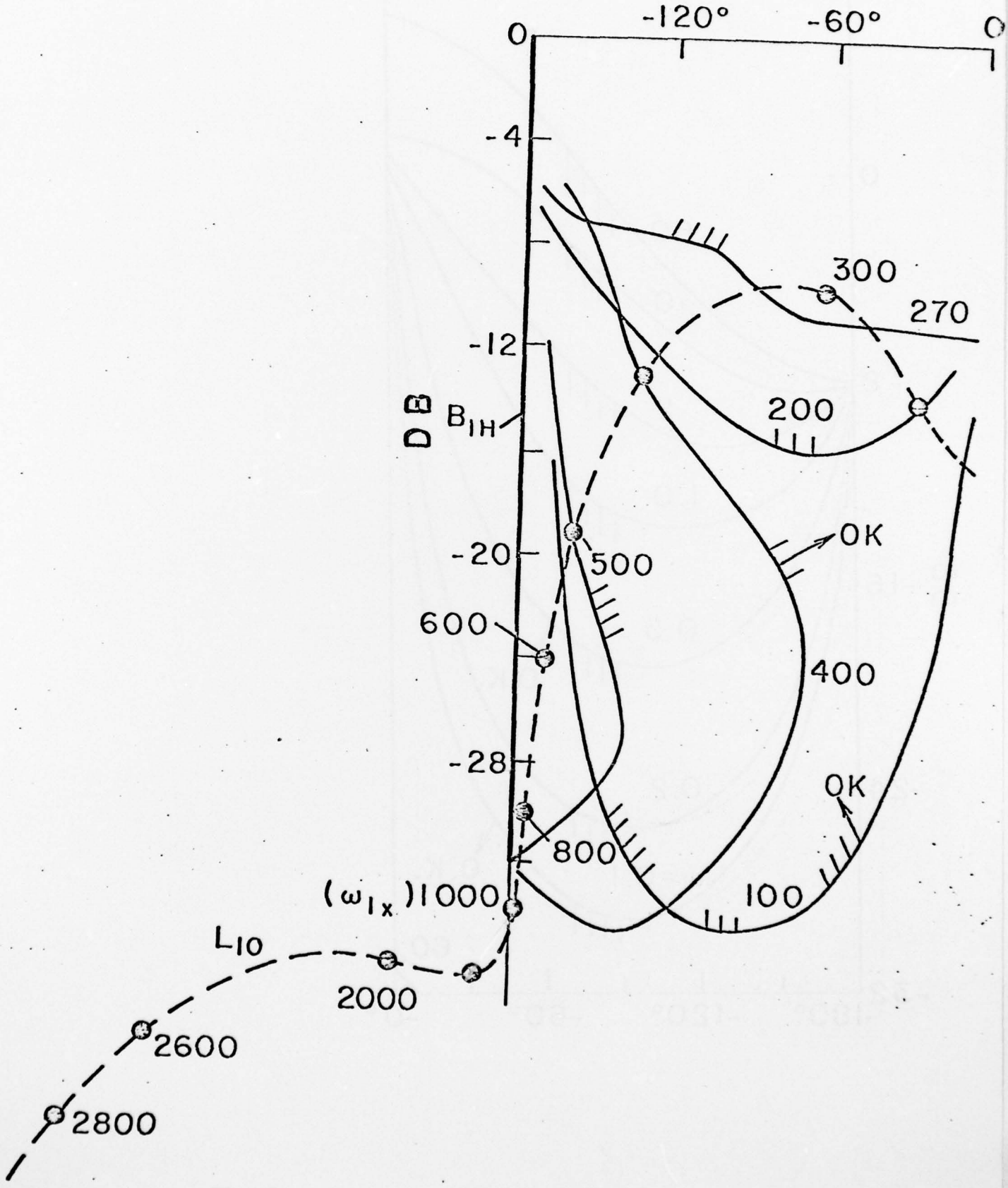

Fig. 6b Bounds $B_1(\omega)$ on $L_{10}(j\omega)$ in I_B, I_C - lower ones in I_B.

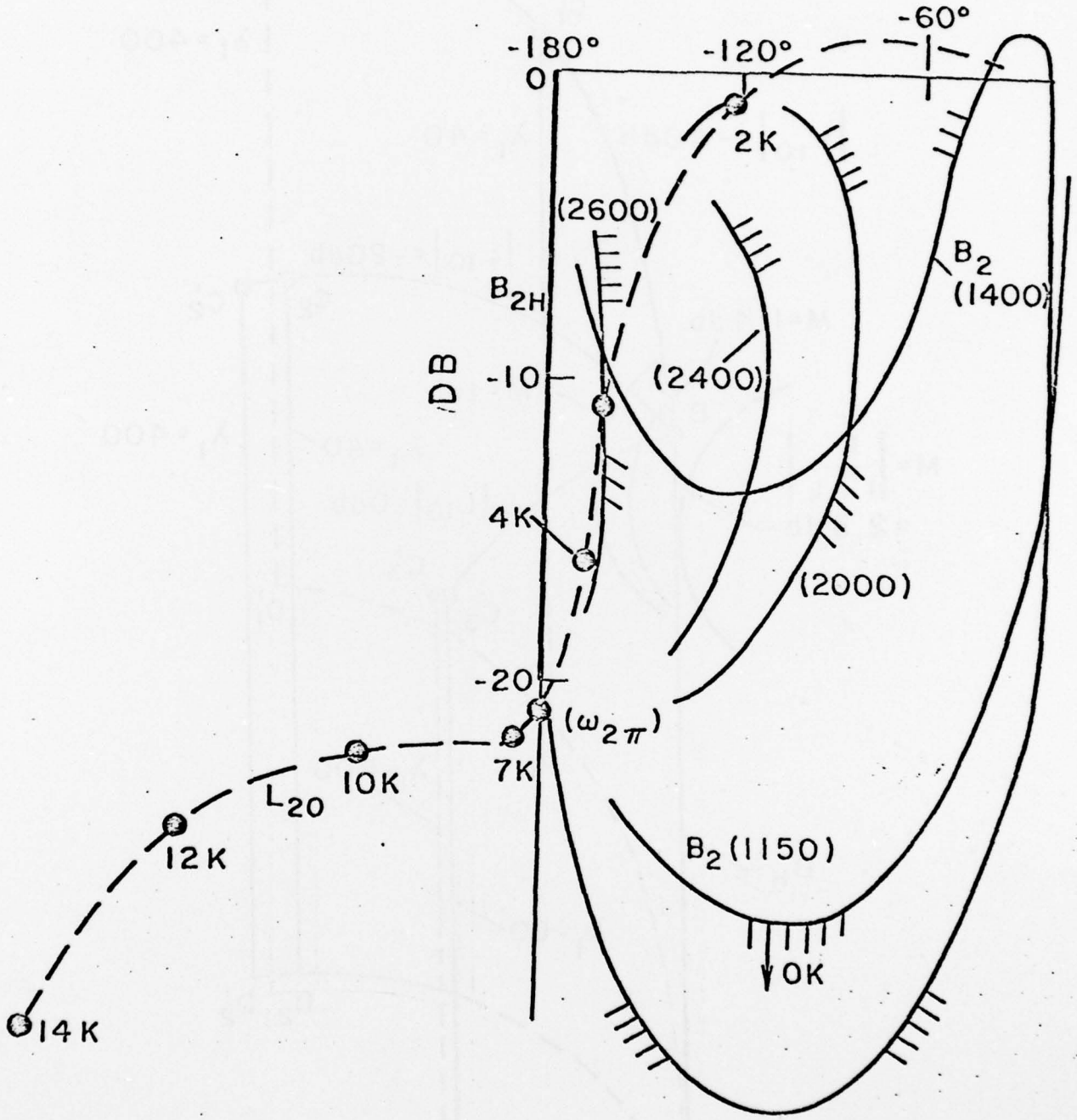

Fig. 7 Bounds $B_2(\omega)$ on $L_{20}(j\omega)$ - upper in I_{1A}.

Arg $L_{10} = -90°$ for various $|L_{10}|$ and λ_1.

Fig. Ala.

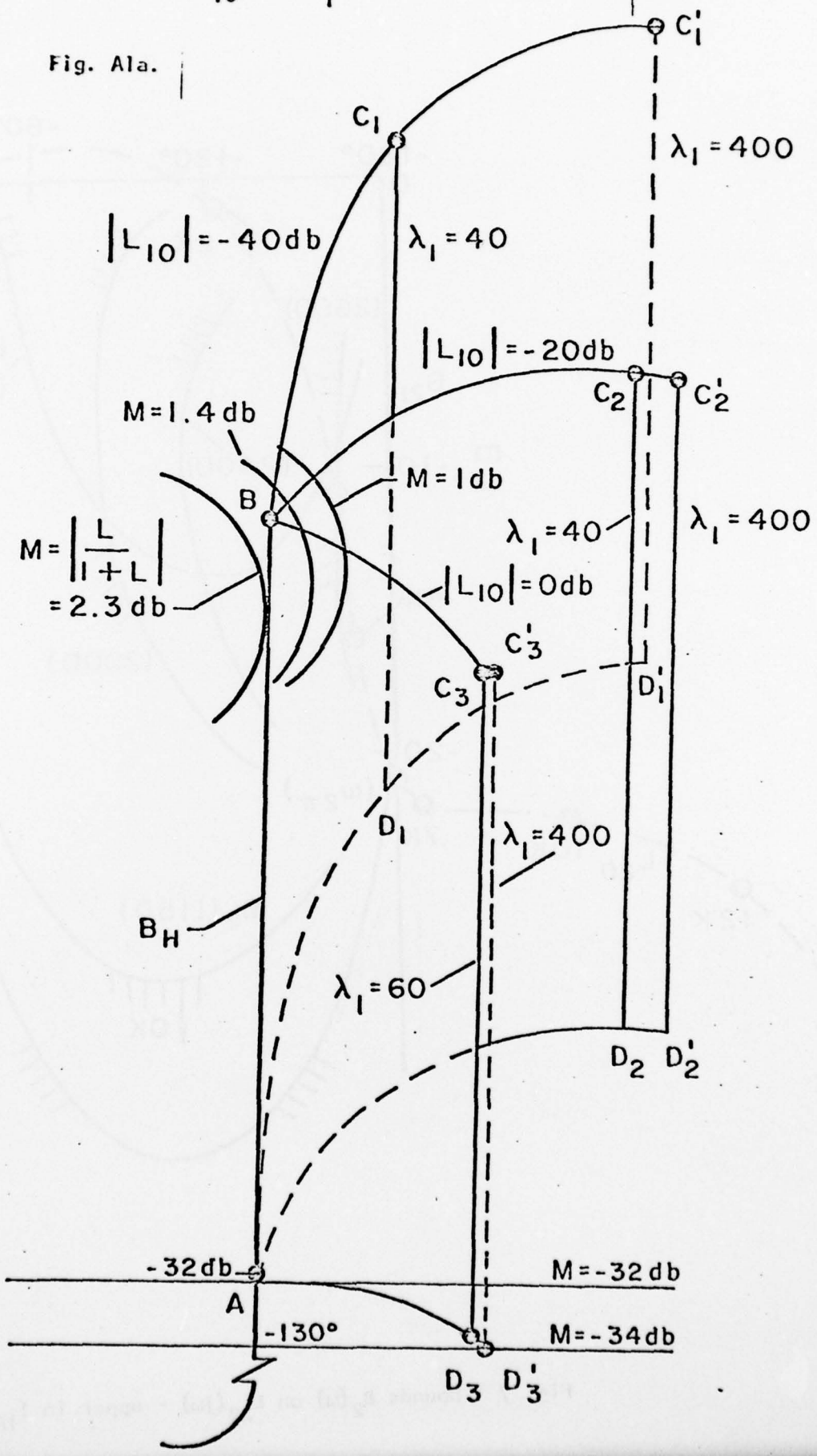

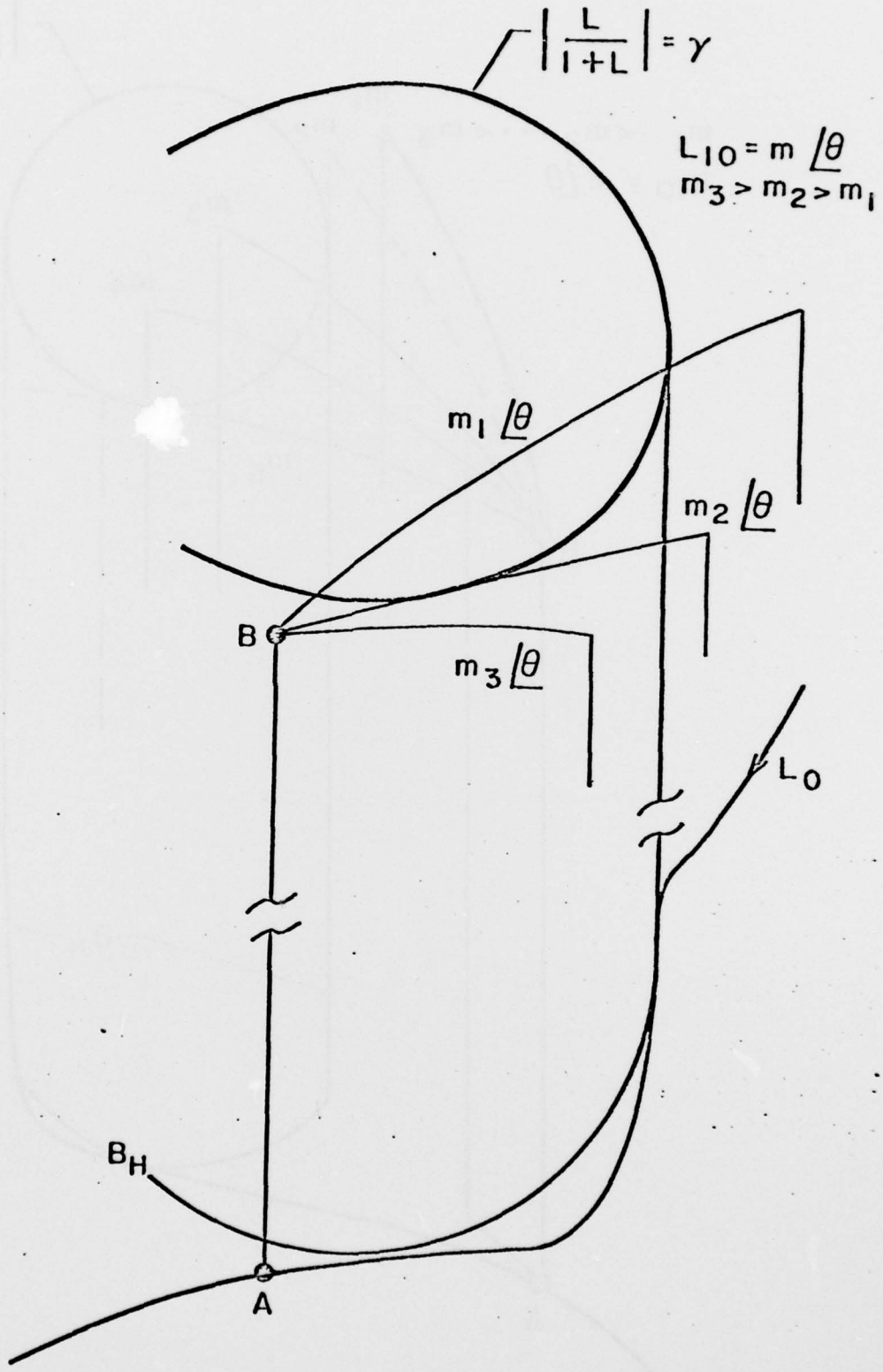

Fig. A1b. Explanation of nature of $B_1(\omega)$ in l_B - family of γ^1 at fixed Arg $L_{10} = 0$.

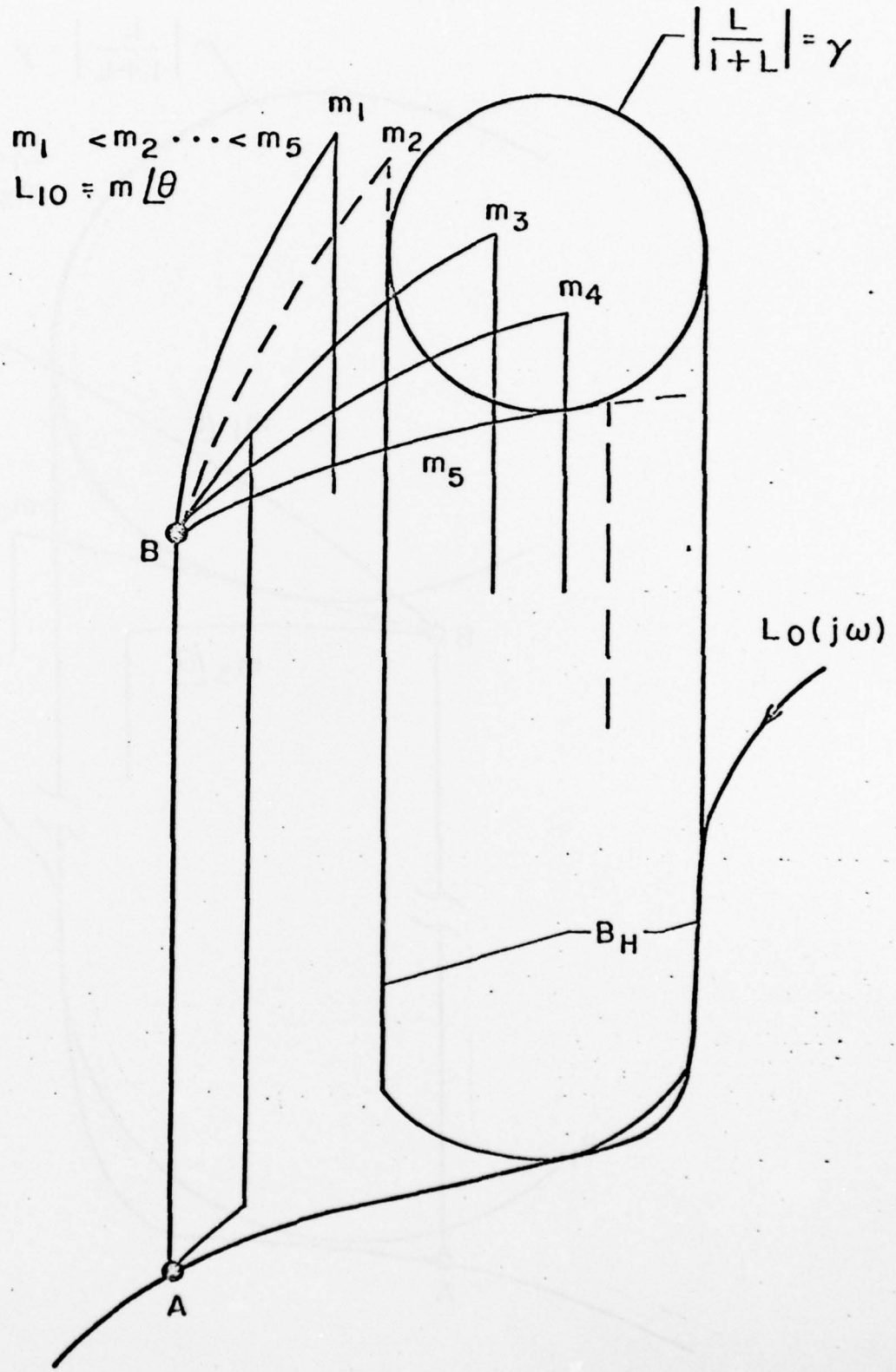

Fig. A1c. Explanation of nature of $B_1(\omega)$ in I_C. At Arg $L_{10} = \pi$ $m_2 > |L_{10}|_{ok} > m_5$.

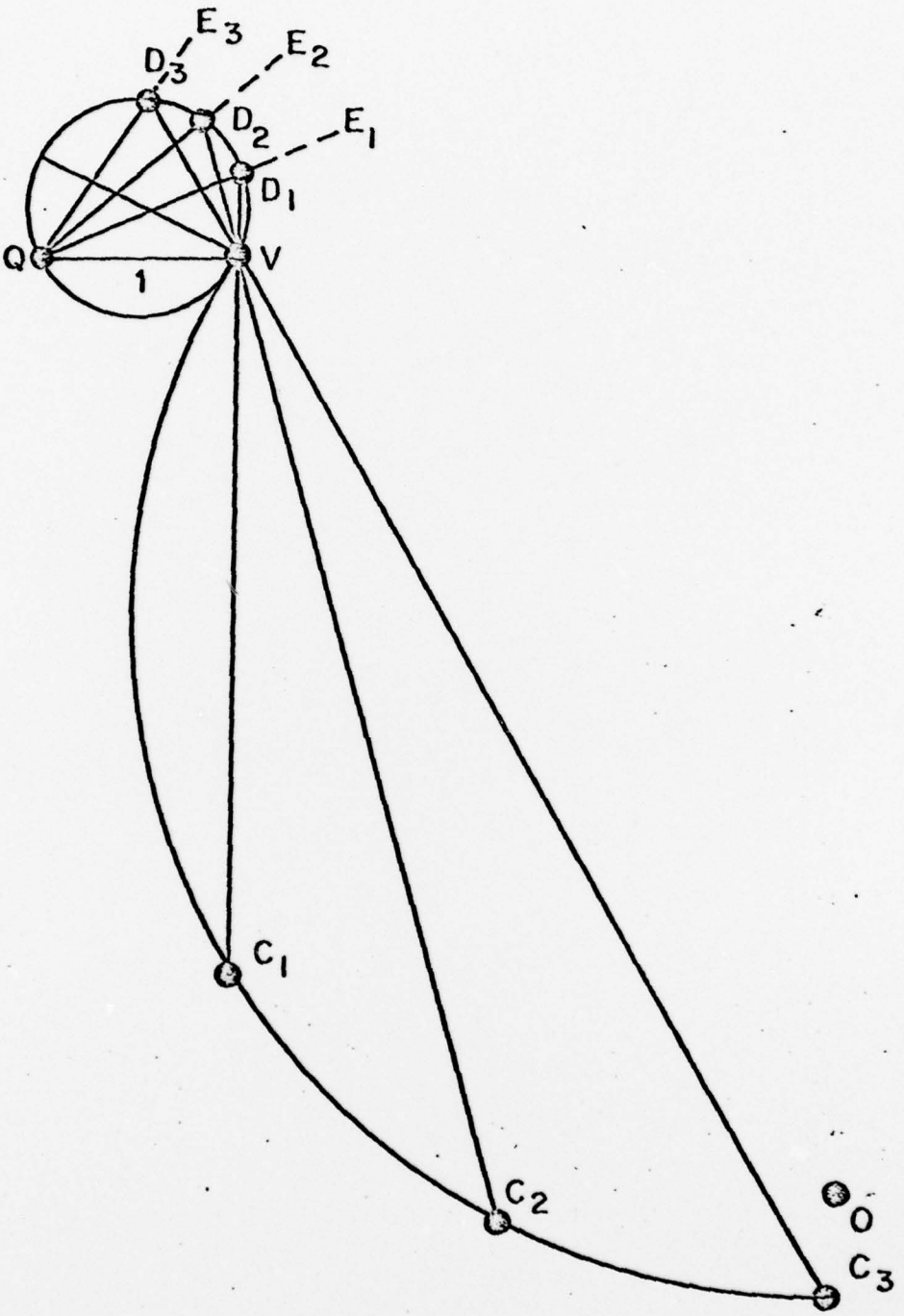

Fig. A2 Explanation of nature of $B_2(\omega)$ in I_{1C}.

SECURITY CLASSIFICATION OF THIS PAGE (When Data Entered)

(19) REPORT DOCUMENTATION PAGE

READ INSTRUCTIONS BEFORE COMPLETING FORM

1. REPORT NUMBER (18) AFOSR-TR-77-1222	2. GOVT ACCESSION NO.
3. RECIPIENT'S CATALOG NUMBER (9)	
4. TITLE (and Subtitle) (6) A SYNTHESIS THEORY FOR A CLASS OF MULTIPLE-LOOP SYSTEMS WITH PLANT UNCERTAINTY.	5. TYPE OF REPORT & PERIOD COVERED Interim rept.
	6. PERFORMING ORG. REPORT NUMBER
7. AUTHOR(s) (10) Isaac Horowitz, Te-Shing Wang	8. CONTRACT OR GRANT NUMBER(s) (15) AFOSR-76-2946
9. PERFORMING ORGANIZATION NAME AND ADDRESS University of Colorado, Department of Electrical Engineering, Boulder, Colorado 80309	10. PROGRAM ELEMENT, PROJECT, TASK AREA & WORK UNIT NUMBERS (16) 61102F 2304/A1 (17) A1
11. CONTROLLING OFFICE NAME AND ADDRESS Air Force Office of Scientific Research/NM, Bolling AFB DC 20332	12. REPORT DATE 1977
	13. NUMBER OF PAGES 43
14. MONITORING AGENCY NAME & ADDRESS (if different from Controlling Office) (11) 1977 (12) 49p.	15. SECURITY CLASS. (of this report) UNCLASSIFIED
	15a. DECLASSIFICATION/DOWNGRADING SCHEDULE

16. DISTRIBUTION STATEMENT (of this Report)

Approved for public release; distribution unlimited.

17. DISTRIBUTION STATEMENT (of the abstract entered in Block 20, if different from Report)

18. SUPPLEMENTARY NOTES

19. KEY WORDS (Continue on reverse side if necessary and identify by block number)

20. ABSTRACT (Continue on reverse side if necessary and identify by block number)

There is given a single input-output linear, time-invariant plant with large parameter uncertainty consisting of two parallel branches, one of which has n internal sensing points. The objective is to satisfy specified frequency domain bounds on the

DD FORM 1 JAN 73 1473 EDITION OF 1 NOV 65 IS OBSOLETE

UNCLASSIFIED

SECURITY CLASSIFICATION OF THIS PAGE (When Data Entered)

20. ABSTRACT (Continued)

system response to commands and disturbances over the parameter range, and to do so with sensibly minimum net effect at the plant input, of the n + 1 sensor noise sources. The basic problem is how to best divide the feedback burden among the n + 1 available feedback loops L_i. The procedure developed has high transparency, giving early perspective on the loop bandwidths, permitting approximate loop trade-offs without a detailed design. While the development is more difficult than in the single cascaded plant system, the procedure and final results are very similar: Each L_i has only one distinct frequency range say ω_i, in which there is trade-off between L_i and L_{i+1}, and $\omega_{i+1} > \omega_i$ with steadily increasing loop bandwidths going backwards from plant output to input. It is shown that for a class of problems the sensor noise effects can be tremendously reduced, when compared to an optimum single-loop design satisfying the same specifications.